

# Deep learning in ultrasound elastography imaging: A review

Hongliang Li<sup>1,2</sup> | Manish Bhatt<sup>1</sup> | Zhen Qu<sup>1</sup> | Shiming Zhang<sup>3</sup> |  
Martin C. Hartel<sup>3</sup> | Ali Khademhosseini<sup>3</sup> | Guy Cloutier<sup>1,2,4</sup>

<sup>1</sup>Laboratory of Biorheology and Medical Ultrasonics, University of Montreal Hospital Research Center, Montréal, Québec, Canada

<sup>2</sup>Institute of Biomedical Engineering, University of Montreal, Montréal, Québec, Canada

<sup>3</sup>California Nanosystems Institute, University of California, Los Angeles, Los Angeles, California, USA

<sup>4</sup>Department of Radiology, Radio-Oncology and Nuclear Medicine, University of Montreal, Montréal, Québec, Canada

## Correspondence

Guy Cloutier, Laboratory of Biorheology and Medical Ultrasonics, University of Montreal Hospital Research Center, Montréal, QC, Canada.

Email: [guy.cloutier@umontreal.ca](mailto:guy.cloutier@umontreal.ca)

## Funding information

Canadian Institutes of Health Research, Grant/Award Numbers: 399544, 273738, 301520, 134748; Fonds de Recherche du Québec, Grant/Award Number: 2019-AUDC-263591; Natural Sciences and Engineering Research Council of Canada, Grant/Award Number: 462240-14

## Abstract

It is known that changes in the mechanical properties of tissues are associated with the onset and progression of certain diseases. Ultrasound elastography is a technique to characterize tissue stiffness using ultrasound imaging either by measuring tissue strain using quasi-static elastography or natural organ pulsation elastography, or by tracing a propagated shear wave induced by a source or a natural vibration using dynamic elastography. In recent years, deep learning has begun to emerge in ultrasound elastography research. In this review, several common deep learning frameworks in the computer vision community, such as multilayered perceptron, convolutional neural network, and recurrent neural network, are described. Then, recent advances in ultrasound elastography using such deep learning techniques are revisited in terms of algorithm development and clinical diagnosis. Finally, the current challenges and future developments of deep learning in ultrasound elastography are prospected.

## KEYWORDS

artificial intelligence, deep learning, elastography, ultrasound

## 1 | INTRODUCTION

Changes in the mechanical properties of tissues are associated with the onset and progression of some diseases. For example, liver fibrosis is associated with increased liver tissue stiffness, and manual palpation has been used for centuries by physicians to compress an organ and feel its stiffness for disease diagnosis. However, interpreting palpation remains subjective to physicians. Ultrasound elastography seeks to objectively characterize tissue stiffness using ultrasound imaging. Specifically, tissue deformation is induced by internal or external vibrations. Then, the response of the tissue deformation is captured by ultrasound images from which elastography techniques can derive information on tissue stiffness. Approaches were also instrumented to assess tissue viscosity using ultrasound.

Ultrasound techniques for mechanical tissue assessment have been very actively studied over the years and can be divided into two groups: quasi-static and dynamic elastography. The quasi-static methods can determine the elasticity or Young's modulus  $E$  by measuring the strain  $\epsilon$  caused by known compressive force  $\sigma$  and the area of such force. As it is challenging to measure the compressive force locally at the site of deformation, scientists usually only measure the strain to provide contrast in terms of relative stiffness.<sup>1-4</sup> As an alternative in quasi-static elastography, the natural pulsation of an organ is often used and strain  $\epsilon$  is measured to assess its rigidity.<sup>5-9</sup> Dynamic methods in elastography can determine the complex shear modulus from which the elasticity  $E$  and viscosity  $\eta$  can be derived by tracing and analyzing a propagated shear wave (SW) into the specimen. As the shear modulus of various

tissues spans over orders of magnitude, dynamic methods provide high contrast among different tissues/organs regarding their mechanical properties. The source of vibration in SW elastography (SWE) can be external (actuator),<sup>10</sup> internal (radiation pressure),<sup>11,12</sup> or natural (e.g., SWs produced by closing heart valves).<sup>13–15</sup>

In recent years, deep learning has been widely developed by the computer vision community.<sup>16–19</sup> However, the application of deep learning to analyze medical images is not straightforward. One reason is that the labeled medical data for training is not as readily available as computer vision images due to the higher costs and professional workload needed for their procurement. Ethical regulatory issues for use of medical images also have to be considered. In addition, medical images are more complex and less interpretable than scenic images. In the case of ultrasound, the inter- and intra-observer variabilities limit the clinical diagnosis capabilities using deep learning. Consequently, additional efforts have been devoted to ultrasound elastography research.

Challenges specific to elastography are required because state-of-art strain reconstruction algorithms are model based, which may induce implicit model errors, and SWE methods rely on mechanical assumptions on tissue properties increasing variance when the underlying tissue differs from expected properties. One may expect that data-driven deep learning would reduce model bias and variance. In recent years, reviews have been made available on deep learning applications for ultrasound beamforming, Doppler ultrasound imaging, and ultrasound localization microscopy,<sup>20</sup> and on advances in deep learning for classification, detection, and segmentation of ultrasound images.<sup>21</sup> To our knowledge, there is no literature review on deep learning applied to ultrasound elastography imaging. In this review, recent advances using deep learning techniques are presented, with a focus on algorithm developments and clinical diagnostic results. A summary of ultrasound strain and SW-based elastography methods is also presented to introduce readers to this field.

The rest of the paper is divided into four sections: (1) an overview of ultrasound elastography, (2) an overview of deep learning techniques used in ultrasound elastography, (3) a literature review on the applications of deep learning in ultrasound elastography, and (4) a summary and perspectives.

## 2 | ULTRASOUND ELASTOGRAPHY TECHNOLOGIES

### 2.1 | Quasi-static elastography

Quasi-static elastography, also called strain imaging, measures the tissue strain under a stress induced by a

compression and/or a relaxation. The first work on strain imaging utilized a manual compression on the top of a tissue to induce its deformation.<sup>1</sup> The schematic and concept of strain imaging is shown in Figure 1. Here, an ultrasound transducer uniaxially applies a small compression on a soft phantom with a hard inclusion. The deformation process of the phantom can be regarded as the compression of a spring, where the parts with different stiffnesses give rise to different displacements according to Hooke's law. As the stress  $\sigma$  may not be measured in practice, the absolute value of  $E$  may not be determined. Instead, a relative stiffness is determinable, that is, higher  $\varepsilon$  represents softer whereas lower  $\varepsilon$  represents stiffer materials. To measure these displacements at each depth, a cross-correlation method is usually applied to analyze two radio-frequency (RF) or in-phase and quadrature (I/Q) echoes, namely, pre- and post-compression signals. The position that provides the largest value in a cross-correlation map determines the displacement between pre- and post-compression signals. Finally, the spatial gradient of the displacement field represents the strain distribution, which is also known as an elastogram. For two-dimensional (2D) ultrasound scan, 2D strain estimations can be obtained using the normalized cross-correlation (NCC):

$$NCC(i, j) = \frac{\sum_{y=0}^{M-1} \sum_{x=0}^{N-1} (r(x, y) - \bar{r}) (t(x+i, y+j) - \bar{t}(i, j))}{\sqrt{\sum_{y=0}^{M-1} (r(x, y) - \bar{r})^2 \sum_{x=0}^{N-1} (t(x+i, y+j) - \bar{t}(i, j))^2}}, \quad (1)$$

where  $r$  and  $t$  are pixel intensities from pre- and post-compression images, respectively, and  $\bar{r}$  and  $\bar{t}$  are mean pixel intensities inside measurement windows with size of  $M \times N$ . The position of the peak of a 2D NCC map determines the displacement vector of the centroid of a measurement window. With a quasi-static measurement, tissue viscosity can also be determined by knowing the elasticity and measuring the relaxation time of the tissue from the compressive force.<sup>2,22,23</sup>

Other approaches were used in quasi-static elastography. Strain of the cardiac muscle was measured with the natural cardiac pulsation as the mechanical stimulus, which is referred to myocardial elastography.<sup>24</sup> Quasi-static elastography was also explored to characterize the vessel wall with intravascular ultrasound images. The natural cardiac pulsation or the inflation of a compliant balloon on a catheter was used to differentiate the coronary calcified plaque component (less strain) from noncalcified tissues (higher strain) in vivo.<sup>25,26</sup> Noninvasive vascular elastography (NIVE) was also proposed for determining the stability or vulnerability of an atherosclerotic plaque using ultrasound imaging.<sup>8</sup> In the latter study, instead of using an NCC method, an affine model-based algorithm was proposed to estimate strains directly without computing gradients

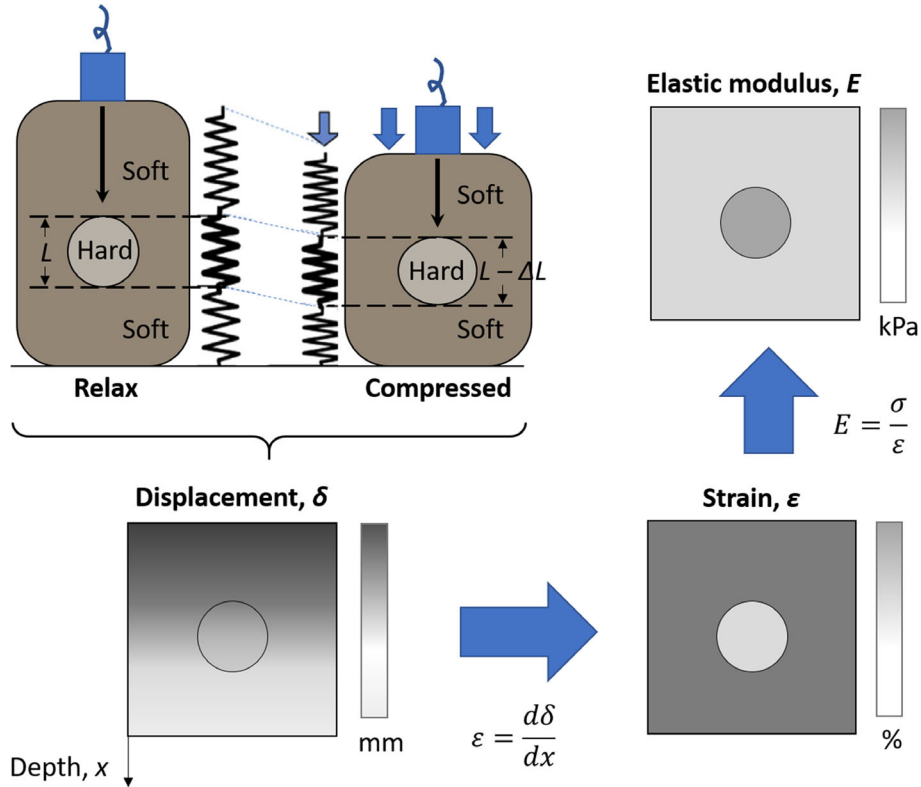


**FIGURE 1** Principle of ultrasound strain imaging. A minute compression is applied on a soft phantom with a hard inclusion. Two radio-frequency (RF) echoes, described as pre- and post-compression signals, are acquired and analyzed to obtain displacements at each depth. Finally, the spatial gradient of the displacement field represents the strain distribution, which indirectly represents the elastic modulus distribution.

of displacements. Specifically, in the framework of the Lucas–Kanade optical flow (OF) equation,  $[I_x \ I_z] \begin{bmatrix} U_x \\ U_z \end{bmatrix} = -I_t$ , where  $I_x$ ,  $I_z$ ,  $I_t$  are the derivatives of the image intensity in the corresponding direction and time, a Lagrangian speckle model estimator was developed to directly obtain affine motion components, including displacements, strains, and shears,<sup>8,27</sup> as shown in the following equation:

$$\begin{bmatrix} I_x & I_x & I_x & I_x & I_x & I_x \\ I_x & I_x & I_x & I_x & I_x & I_x \\ I_x & I_x & I_x & I_x & I_x & I_x \\ I_x & I_x & I_x & I_x & I_x & I_x \\ I_x & I_x & I_x & I_x & I_x & I_x \\ I_x & I_x & I_x & I_x & I_x & I_x \end{bmatrix} \begin{bmatrix} s_{xx} \\ s_{xz} \\ U_x \\ s_{zx} \\ s_{zz} \\ U_z \end{bmatrix} = -I_t, \quad (2)$$

where  $U_x$ ,  $U_z$ ,  $s_{xx}$ ,  $s_{xz}$ ,  $s_{zx}$ , and  $s_{zz}$  stand for lateral displacement, axial displacement, lateral strain, lateral shear, axial shear, and axial strain, respectively. NIVE could determine the strain field of the moving vessel wall of a superficial artery (e.g., the carotid) caused by the natural cardiac pulsation without the need of an external compression. This method was also introduced to study normal vessel walls.<sup>28</sup> Recently, the same

group proposed a sparse model strain estimator in the framework of the Horn and Schunck OF method.<sup>29</sup> It formulates strain estimations as an optimization problem, where a cost function incorporating a data term and a regularization term was minimized as follows:

$$\min_{U_x, U_z} D_{data}(U_x, U_z) + \lambda_1 R_{smooth}(U_x, U_z) + \lambda_2 R_{incomp}(U_x, U_z), \quad (3)$$

where  $D_{data}(\cdot)$  represents the data term in the OF equation,  $R_{smooth}(\cdot)$  is a regularization term that ensures spatial smoothness of displacement,  $R_{incomp}(\cdot)$  is another regularization term representing tissue incompressibility, and  $\lambda_1$  and  $\lambda_2$  are parameters to control the influence of the regularization terms. This method was able to estimate a dense strain field at a high resolution and high computation efficiency.<sup>29</sup>

Due to the limited lateral resolution of ultrasound images compared with the axial resolution, the motion in the lateral direction is challenging to track in strain elastography. Angular compounding,<sup>7</sup> coherent plane wave compounding imaging,<sup>27</sup> and synthetic aperture imaging<sup>6</sup> were proposed to enable more accurate lateral estimations, respectively. Out-of-plane motion

is another potential factor causing estimation artifacts in the context of NIVE.<sup>30</sup> In addition, it is not easy to perform 2D estimations in the frequency domain as lateral phase information is not available as there is no carrier frequency in the lateral direction with conventional ultrasound images. As an alternative, a dedicated transverse oscillation image reconstruction method<sup>31,32</sup> can be used for image reconstruction before strain estimations, as in Ref. [33].

## 2.2 | Dynamic elastography

Dynamic elastography uses SW measurement methods to determine the tissue viscoelasticity by tracing and analyzing the propagating wave into the specimen; an exhaustive review on SW elastography can be found in Refs. [34–37]. SWs, also called transverse waves, are moving mechanical waves that consist of particle oscillations occurring perpendicular to the direction of the energy transfer. In a viscoelastic material, the SW propagation equations are given by<sup>38</sup>

$$\rho \frac{\partial^2 u_i}{\partial t^2} - \mu \nabla^2 u_i = 0, \quad (4)$$

$$\mu = G' + jG'', \quad (5)$$

where  $\rho$  is the density of the specimen,  $u_i$  is the particle displacement occurring in the  $i$  direction, and  $t$  is time.  $\nabla^2 u_i$  is the spatial Laplacian of the particle displacement. The parameter  $\mu$  is the second Lamé coefficient and it denotes the shear viscoelasticity represented by the shear storage and loss moduli,  $G'$  and  $G''$ , respectively, in which  $G'$  reflects the elastic property and  $G''$  the viscous response.

Alternatively, a material mathematical model, such as Voigt model that is represented by a purely elastic spring connected in parallel to a purely viscous damper, is frequently used to directly describe viscoelastic materials. Based on the Voigt model,  $G'$  and the viscosity  $\eta$  have the following relationship with the velocity  $v_S$  and the attenuation  $\alpha_S$  of the SW, where  $\omega_S$  represents the angular frequency of the SW<sup>39</sup>:

$$G' = \frac{\rho \omega_S^2 v_S^2 \cdot (\omega_S^2 - \alpha_S^2 v_S^2)}{(\omega_S^2 + \alpha_S^2 v_S^2)^2}, \quad (6)$$

$$\eta = \frac{\rho \omega_S^2 v_S^2 \cdot 2\alpha_S v_S}{(\omega_S^2 + \alpha_S^2 v_S^2)^2}. \quad (7)$$

It is worth noting that for a soft biological tissue, the elastic property dominates the tissue mechanical

property and the viscous behavior is often neglected. Therefore, in such case, it is considered a purely elastic material, and  $\alpha_S$  could be ignored, so that a specific material model is not necessarily required and thus  $G'$  can be expressed by

$$G' = \rho v_S^2. \quad (8)$$

When the viscosity  $\eta$  is taken into account for the tissue characterization, according to Equation (7), it can be determined either using both  $v_S$  and  $\alpha_S$ , or alternatively by evaluating the dispersion of  $v_S$  with respect to  $\omega_S$  without determining the value of  $\alpha_S$ , that is, solving Equation (8) by knowing multiple pairs of  $v_S$  and  $\omega_S$ .<sup>40</sup> Alternatively, if no rheological model is assumed (e.g., the Voigt model), it may be more convenient to assess the shear storage  $G'$  and loss  $G''$  moduli to describe the mechanical property of the tissue.<sup>41</sup> This is particularly relevant considering the fact that the simple Voigt model might not allow mimicking both normal and pathological tissues of different grades of disease severity.

The dynamic methods mainly derive the viscoelastic parameters according to Equations (4)–(8), by tracing and analyzing the SW propagation in a specimen of interest. In 1988, Lerner et al. proposed a method to map the propagation of a low-frequency continuous SW with a Doppler ultrasound displacement detection technique,<sup>42</sup> and such an image of the SW displacement could reflect the tissue stiffness. Later in 1990, Yamakoshi et al. proposed a measurement method using an external mechanical vibration source, and  $v_S$  was determined by analyzing the wavelength of a continuously propagated SW through an ultrasound Doppler technique.<sup>43</sup> Instead of measuring continuous SWs, Catheline et al. developed in 1999 an impulse SW measurement method, which used a high frame-rate ultrasound imaging system to trace the wavefront of the transient SW produced by a mechanical vibrator.<sup>10</sup> Indeed, conventional focused ultrasound systems are triggering transducer elements sequentially from one side of the image to the other side producing a frame-rate of typically below 100 frames/s, which is not sufficient for SW tracking. The development of plane wave beamforming allowed implementing SW imaging methods more efficiently. With this method, a plane wave system triggers all transducer elements of the probe at the same time to emit a plane wavefield, enabling it to have a high frame rate (more than 1000 frames/s and up to 10,000 frames/s).<sup>12</sup> Using this approach,  $v_S$  is determined through a time-of-flight technique by measuring the time elapse of the impulse SW to travel through two locations with a known distance. As such a method uses impulse SW, it is also called transient SW imaging, or transient elastography.

The SW excitation can also be made inside the specimen by means of an ultrasound radiation force (or acoustic radiation force, ARF) technique.<sup>11,38,44–48</sup>

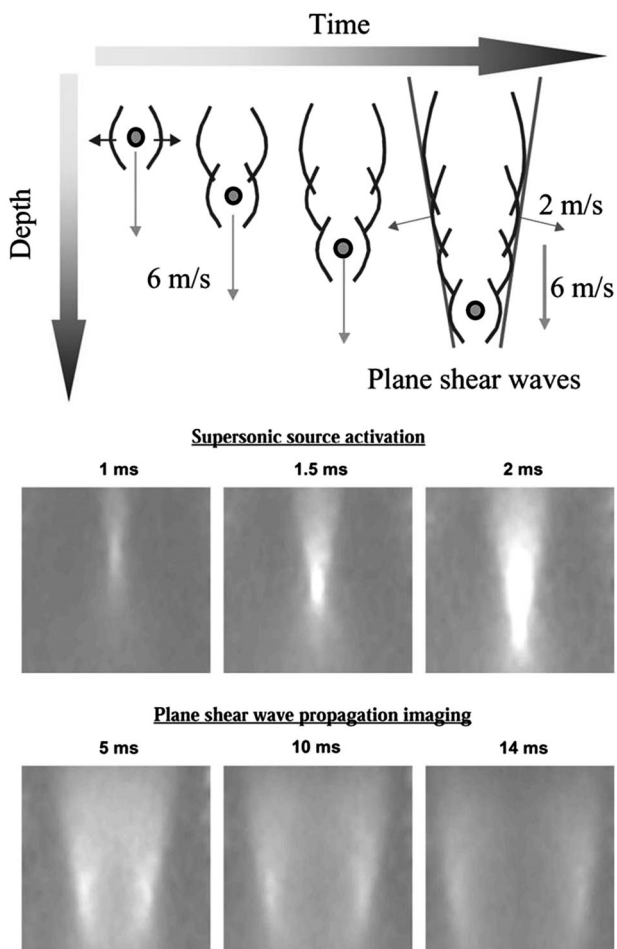


**FIGURE 2** Generation of supersonic plane shear waves. Source: Reproduced with permission from Ref. [12].

Among all, the supersonic shear imaging (SSI) technique<sup>12</sup> is considered the most advanced SW measurement method. With this method, the ultrafast plane wave imaging method is used to track multiple ARF impulses that are excited consecutively and very quickly at different depths. Each excitation produces a point source-like SW, which then interferes constructively and results in two SW planes propagating in the opposite directions, as can be seen in Figure 2. By using the ultrafast scanner to trace these SWs, a 2D SW speed image of  $v_S$  can be obtained. Moreover, as this technique creates broadband SWs, tissue viscosity can also be estimated through the  $v_S$  dispersion method.<sup>45</sup>

### 2.3 | Clinical applications and limitations

Over the past several years, many notable methods have been validated with different clinical datasets to diagnose several organ dysfunctions. Elastography techniques (both quasi-static and SW-based) were also integrated into commercial ultrasound equipment for

clinical diagnosis. As extensive review papers have addressed the clinical applications of ultrasound elastography, a brief review is given later. Clinically oriented overviews can be found in Refs. [35, 36, 49–51]. Table 1 concisely summarizes some clinical applications of ultrasound elastography with popular techniques.

Breast cancer imaging is the most common use of strain imaging. It is a qualitative technique to characterize benign and malignant breast masses. There are three typical parameters to interpret strain images<sup>35,51</sup>: (1) elastogram to B-mode length ratio (EI/B ratio); (2) 5-point color scale (Tsukuba score); and (3) fat-to-lesion ratio (strain ratio). A meta-analysis, including 12,398 lesions (4242 malignant), showed a high sensitivity of EI/B ratio at 96%. The highest specificities of the EI/B ratio and 5-point color scale are 88% and 87%, respectively.<sup>67</sup> One limitation of breast strain imaging is that the amount of compression stress for optimal strain maps varies for different vendors, which requires a learning curve for each ultrasound system.<sup>51</sup>

For prostate cancer, strain imaging has shown superiority over transrectal ultrasonography (TRUS). Several studies reported strain imaging achieving sensitivities of 62%–72%, and specificities of 71%–79% for prostate cancer detection.<sup>52–54</sup> Therefore, targeted TRUS biopsy along with strain imaging has potential to reduce the number of biopsy samples.<sup>35</sup>

Thyroid nodule characterization is another area that has shown strain imaging to be potentially helpful. A meta-analysis with 8 studies, including a total of 639 thyroid nodules, showed overall a mean sensitivity and a mean specificity for detecting malignant thyroid nodules of 92% and 90%, respectively.<sup>55</sup> A recent multicenter study concluded that a combination of the thyroid imaging reporting and data system (TI-RADS) with strain imaging could provide a higher sensitivity than using TI-RADS criteria alone.<sup>56</sup>

SW elastography was used to evaluate liver stiffness and diagnose patients with liver fibrosis and steatosis.<sup>48,57</sup> Breast SW elastography could also provide quantitative information on breast lesions, which was widely applied to diagnose breast cancer.<sup>58,59</sup> Dynamic elastography has also been shown as a good complementary method to detect the lesion area in prostate cancer.<sup>60</sup> When the lesion is identified, elastography may help clinicians make decisions on whether to carry out a biopsy in the lesion area. Additionally, dynamic elastography has been employed to differentiate thyroid cancers by evaluating the tissue stiffness.<sup>61</sup> Other applications, such as the characterization of the musculoskeletal system,<sup>62</sup> tendon,<sup>63,64</sup> lymph nodes,<sup>65</sup> and many other organs,<sup>66,68–70</sup> have also shown good results that reflect differences between normal and abnormal tissues.

At present, improving the measurement precision and accuracy of existing techniques is always an

**TABLE 1** Summary of clinical applications using ultrasound elastography

Classification	Clinical applications	Advantages	Limitations
Quasi-static elastography (strain imaging)	Breast cancer <sup>35,51</sup> Prostate cancer <sup>52–54</sup> Thyroid cancer <sup>55,56</sup>	Good sensitivity and specificity; reliable as a screening tool; relatively inexpensive	Assessment is qualitative or semiquantitative; reproducibility can be impacted by the compression load
Dynamic elastography (SWE)	Liver fibrosis and steatosis <sup>48,57</sup> Breast cancer <sup>58,59</sup> Prostate cancer <sup>60</sup> Thyroid cancer <sup>61</sup> Musculoskeletal system <sup>62</sup> Tendon <sup>63,64</sup> Lymph node <sup>65</sup> Kidney disease <sup>66</sup>	Provide quantitative elasticity images; multiple ROIs are available; can reach deep body areas	Image artifacts may be present in heterogeneous tissues; depend on tissue anisotropy

Abbreviations: ROI, region-of-interest; SWE, shear wave elastography.

interesting and active topic. Model-based elastogram reconstruction algorithms may be susceptible to bias and variance arising due to measurement noise, heterogeneous tissue properties, or external exerted pressure. Some model-based strain estimates in strain imaging only provide optimal performances in a range of exerted pressures or motions as they are using specific physical or mathematical modeling.<sup>71,72</sup> SWE methods also rely on mechanical assumptions of “ideal” models (such as homogeneity of a tissue). However, it is well known that muscular tissues are anisotropic, and their inhomogeneity may result in outliers when estimating SW speed or attenuation. Data-driven deep learning methods trained on a large dataset could learn to remove outliers and may overcome bias and variance in such algorithms. Additionally, in model-based algorithms, data-dependent learned regularization could improve reconstructed elastogram quality.

Generally speaking, solving the inverse problem of tissue elasticity computation in an accurate and computationally efficient manner can be more challenging compared to the forward problem of computing the tissue deformation field. The estimation of elasticity often requires a minimization of the differences between the predicted and observed deformation fields, which is often treated as an optimization task in conventional methods, such as the adjoint weighted approach, and solving a nonlinear optimization problem can be costly in practice.<sup>73</sup>

Another limitation of elastography is to observe differences in elasticity magnitude with different acquisitions from different manufacturers’ systems. This may arise due to varying choices of post-processing methods or acquisition parameters responsible for SW generation, such as the power source, frequency, and focusing depth. This system dependency can be overcome if artificial Intelligence (AI)-based algorithms that are trained on a similar dataset are employed.

In terms of clinical diagnosis, current ultrasound elastography technologies or systems fail to provide

clinicians with suggestions based on elasticity measurements. Deep learning methods trained on data from pathology reports can generate preliminary diagnosis. These supports from deep learning can facilitate radiologist’s clinical decision and improve the quality of care to patients.

### 3 | DEEP LEARNING TECHNOLOGIES

Deep learning models are special kind of artificial neural networks (ANNs) that try to resemble the multilayered human cognition system. Even though ANN was first introduced in 1950, the development of deep learning methods took time primarily due to the lack of computing power and relevant data to train the systems. Deep learning models learn through a series of parameterized nonlinear transformations to perform a desired function. The rudimentary nonlinear transformations can take various forms and may include embedded structural priors. A general introduction to deep learning can be found in Ref. [74]. Recent deep learning approaches have demonstrated comparable results to human performance in some medical imaging tasks. For example, image analysis of structures and abnormalities, tumor classifications, disease categorizations, and even composing preliminary radiology reports can now be handled well by deep learning tools.<sup>20</sup> Previous computer-aided detection systems that were developed in the early 2000s for clinical applications were found to generate more false positives than humans.<sup>75</sup> It is expected that deep learning technology may help overcome the limitations of such systems by providing better detection accuracy.

The majority of the algorithms since 2015 employ supervised learning methods, namely, convolutional neural networks (CNNs),<sup>76</sup> whereas semi-supervised, unsupervised, and reinforcement learning (RL) methods are in increasing trend.<sup>77</sup> The advancements in hardware development and the availability of large labeled datasets (i.e., datasets with known identification)

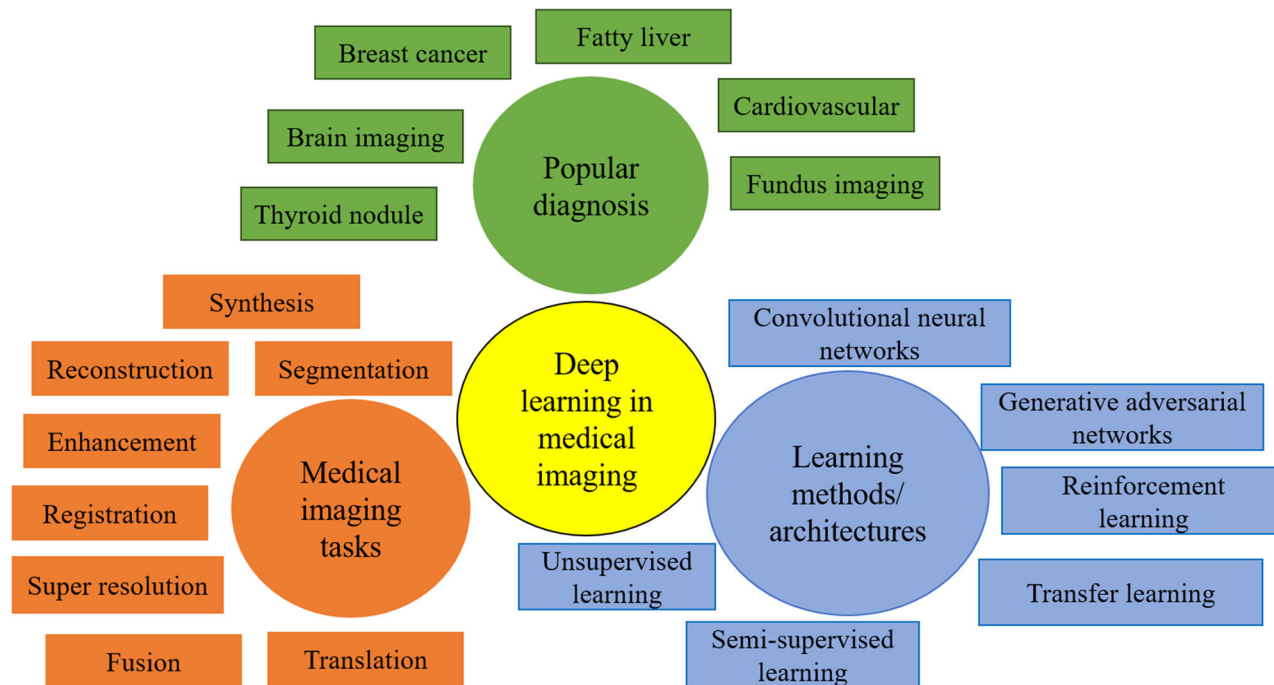


**FIGURE 3** An overview of deep learning in medical imaging. It covers three aspects: the deep learning technologies used in medical imaging (in blue); the medical engineering tasks where deep learning is playing a role (in orange), and specific clinical applications (in green).

resulted in improved CNN performance, encouraging their widespread use in medical imaging. The advantage of a deep neural network is to automatically learn low-level features such as lines or edges and combine them with higher level features such as shapes in the subsequent layers. Krizhevsky et al.<sup>16</sup> introduced several concepts such as rectified linear unit (ReLU) functions in CNNs, data augmentation, and dropouts, which have become dominant architectures used in current medical imaging strategies. Popular deep architectures utilized in medical ultrasound imaging in the last 5 years are briefly introduced in the following subsections. Figure 3 gives an overview of deep learning technologies and their application in medical imaging tasks and clinical decisions.

### 3.1 | Convolutional neural networks

CNNs are the most successful and popular deep learning architecture among supervised learning models in medical imaging due to their ability to preserve spatial relationships when filtering input images. Spatial relationships in medical imaging define tissue interfaces, structural boundaries, or joints between muscle and bone; and thus, CNNs have found special attention. Based on the training strategy, CNNs can be mainly classified in three approaches<sup>78</sup>: (1) patch-based CNNs that train the deep model with image patches and a sliding window approach for testing<sup>79</sup>; however, patch overlap can produce substantial redundancy in training; (2) a

fully convolutional approach that utilizes whole images for training to increase efficiency and avoid redundancy, an example of a modified version of this approach is the U-Net architecture<sup>80</sup>; and (3) the transfer learning approach where a model pretrained on any dataset (to compensate for data deficiency) is applied for medical imaging tasks.<sup>81,82</sup> CNNs have been widely utilized in ultrasound imaging, especially for breast image segmentation tasks. In recent years, U-Net has emerged as one of the most efficient architectures for fast and precise biomedical image segmentations. First designed and applied in 2015, the U-Net architecture is symmetric and consists of a contracting path on the left side (encoder) and an expansive path on the right side (decoder). It has evolved from the traditional CNNs and constitutes a general convolutional process on the contracting path and transposed 2D convolutional layers on the expansive path. Recently, Wildeboer et al.<sup>83</sup> utilized this architecture to generate synthetic SWE maps from B-mode ultrasound images through end-to-end nonlinear mapping. Their network contained direct skip connections on both the encoder filter layer and the decoder layer. The model transferred the encoder layer output across the latent space and then concatenated the large-scale features during decoding. This enabled the deep network to combine fine and course level information to generate high resolution synthetic SW elasticity maps, with less than 10% deviation in the clinically relevant elasticity range.<sup>83</sup> Figure 4 shows the structures of some main deep learning architectures.

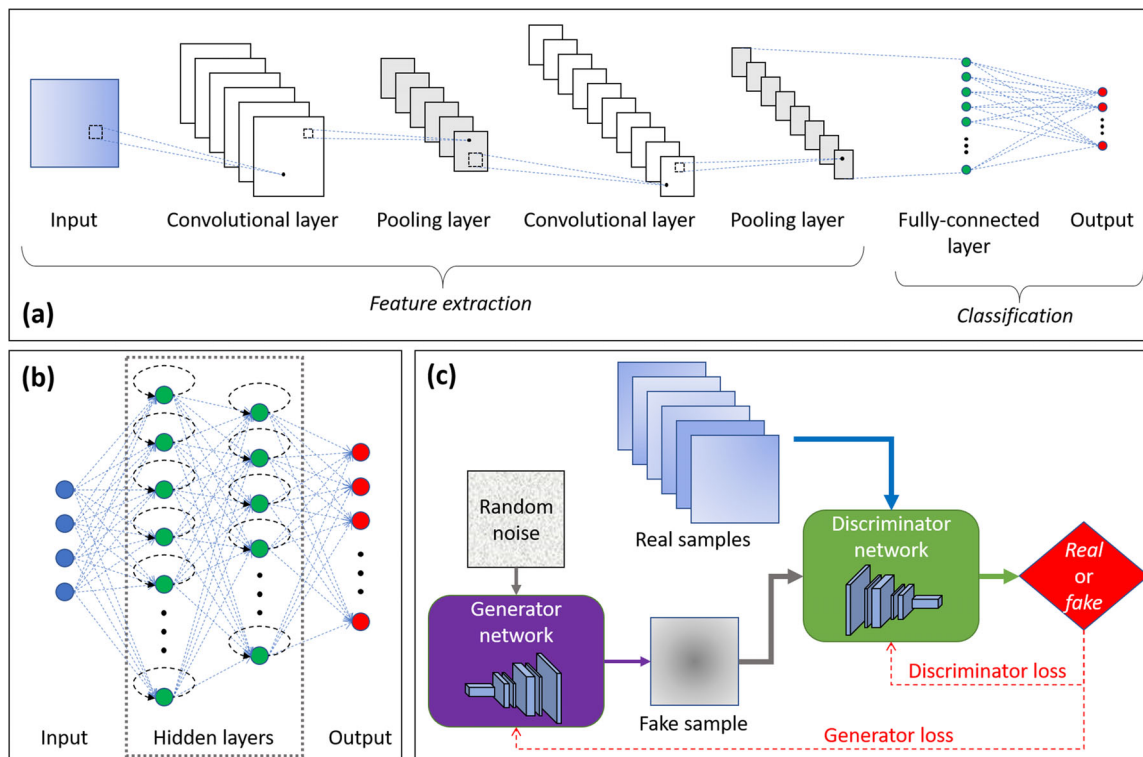


**FIGURE 4** Diagrams of (a) a convolutional neural network (CNN) with two convolutional layers, (b) a recurrent neural network (RNN) with two hidden layers, and (c) a generative adversarial network (GAN), which uses encoder and decoder as its generator and discriminator, respectively.

### 3.2 | Recurrent neural networks

Recurrent neural networks (RNNs), generally considered a type of supervised deep network, are mainly utilized for sequential data analysis, such as in-text or speech processing or data with temporal information. The depth of an RNN can be as long as the input sequence length. The output of a layer in a plain RNN is connected to the next input as well as fed back into the layer itself, resulting in a capacity for contextual “memory.” One of the major applications of RNNs is in image segmentation.<sup>84</sup>

The structural characteristics of the RNN give it an inherent advantage for modeling sequence data.<sup>21,85</sup> RNNs were not widely utilized until recently due to difficulties in training them to capture long-term dependencies. The new modifications of RNNs have evolved into the long short-term memory network and gated recurrent units. These modifications allow holding long-term dependencies or discarding some of the accumulated information.

### 3.3 | Cascaded networks

Deep cascade learning is another approach that splits a deep network into its layers and performs training to fetch a layer until all layers in the input architecture are

well trained.<sup>86</sup> Such a network may have reduced memory and computational time for training compared to the traditional end-to-end backpropagation. Cascaded networks can bypass the vanishing gradient problem by making the network to learn features that have increased correlations with the output on every layer. In addition, even though CNNs are powerful enough to perform one step reconstruction, they can be vulnerable to overfitting especially when training data size is small. A simple solution to overcome this problem is to train a second CNN, which can learn to reconstruct images from the output of the first CNN. Thus, cascading a new CNN to the output of the previous CNN can build extremely powerful deep networks that can iterate between intermediate de-aliasing and data consistency reconstruction. Cascaded CNNs are not yet popular in ultrasound elastography, but one of the first instances of their use in medical image reconstruction was in dynamic MR image reconstruction.<sup>87</sup> In ultrasound elastography, Peng et al. proposed a cascaded CNN model to perform the task of speckle tracking by cascading three small CNNs together and performing multistep training.<sup>88</sup> In the first step, the weights of the first CNN were obtained by leveraging the transfer learning approach (trained on FlyingChairs dataset) and used to initialize the training of the first two cascaded CNNs. In the second step, the weights of the first network were kept fixed and weights of the second

network were updated by training it on a small dataset. In the final step, the weights obtained from the first two cascaded CNNs were used to initialize the training of all three CNNs cascaded together.

### 3.4 | Generative adversarial networks

The first few years of deep learning model development for medical imaging tasks focused on supervised learning. The advent of generative adversarial networks (GANs) opened more applications of generative modeling and new learning in medical image analysis.<sup>89</sup> Generative adversarial networks are a class of deep learning architecture that contains two networks: a generator and a discriminator.<sup>90,91</sup> The generator and discriminator networks are trained jointly with a back-propagation algorithm. The training makes the generative network better at generating more realistic samples, and the discriminator network is better at differentiating artificially generated samples. GANs have been used for several applications in medical imaging, including image synthesis, image reconstruction, image super-resolution, segmentation, and image translation.<sup>92</sup> Image-to-image translation (e.g., for MR to CT, PET to CT) is a new possibility in medical image analysis, and recently MedGAN was proposed as a new end-to-end framework for medical image translation.<sup>93</sup> GANs have been shown to be very effective at synthesizing natural images, and expectedly they have found applications in medical image synthesis too.<sup>94</sup> Those approaches have not yet been applied to the field of ultrasound elastography.

### 3.5 | Advanced learning models

Apart from supervised learning models, some other learning strategies that are also widely used in various imaging tasks are briefly discussed in this section.

Semi-supervised learning models use a small amount of labeled examples and a large amount of unlabeled examples for training the model. These approaches are particularly more helpful in medical imaging tasks as labeled data here is often small in size, challenging to acquire, and expensive. The general approach is to utilize a pretrained network and fine-tune them with either simulation data or labeled data with known ground truth. The learning model can be as simple as a pretrained CNN. Tehrani et al. have shown that a CNN trained on computer vision images and fine-tuned on real ultrasound images could be used for strain imaging in ultrasound elastography.<sup>95</sup> A critical component of semi-supervised learning is to use an efficient loss function, and these authors proposed a novel loss function that combined data loss, smoothness loss,

and consistency loss to make their model learn more efficiently.

Unsupervised learning is another strategy where models are trained using unlabeled datasets, leaving the model on its own to decide similarity and structure in its input. This approach is particularly useful in finding meaningful patterns and groups in the dataset, and for extracting generative features. Unsupervised learning approaches in ultrasound imaging have been used for tasks such as image artifact removal,<sup>96</sup> and image registration and segmentation.<sup>97</sup> Khan et al.<sup>96</sup> proposed an unsupervised deep learning approach based on an optimal transport-driven CycleGAN network for ultrasound image artifact removal. In their model, an unsupervised learning problem was formulated as a stochastic generalization of the penalized least squares using an optimal transport theory.<sup>96</sup> Unsupervised CNNs have been proposed to predict time-delay estimation between RF data in ultrasound elastography. Indeed, Delaunay et al. trained an unsupervised CNN by optimizing a similarity metric between the reference and compressed RF images and added a regularization to improve strain smoothness and preserve displacement continuity.<sup>98</sup>

RL is another approach, which uses an agent that learns by interacting with the surrounding environment to perform a learning task. The agent selects actions and the environment returns a reward or punishment based on the selected action. The goal of the agent is to maximize rewards for perfect learning. RL-based frameworks have been increasingly used in medical imaging for tasks like image registration and image segmentation.<sup>97,99,100</sup> Deep RL has been particularly popular in robotic ultrasound imaging tasks, such as ultrasound guided robotic navigation,<sup>101</sup> video summarization,<sup>102</sup> autonomous navigation of the ultrasound probe,<sup>103</sup> and autonomous robotic systems.<sup>104</sup> However, applications in ultrasound elastography have not yet been demonstrated.

Another key strategy is transfer learning, in which training of the network is performed with a partially related or unrelated dataset along with a labeled training dataset.<sup>105</sup> Tajbakhsh et al.<sup>106</sup> proposed pretraining a CNN on a dataset of labeled natural images and then fine-tune it using medical images. The study reported that a layer-wise fine-tuning scheme could improve the performance of a CNN network for the application at hand based on the amount of available data. Ravishankar et al.<sup>82</sup> observed that the detection performance depended upon the extent of the transfer and their study reported a 20% higher performance with a fine-tuned CNN. One of the main advantages of transfer learning is that it reduces expensive data-labeling efforts. This strategy has also not yet been exploited in the field of ultrasound elastography. Table 2 summarizes main deep learning technologies and architectures.

**TABLE 2** A non-exhaustive list of main deep learning strategies and popular architectures

Algorithms of deep learning	Descriptions
Backpropagation	Used in optimization problem for calculation of gradient; sensitive to noisy data
Stochastic gradient descent	Used to find optimal global minima; avoids trapping in local minima; computationally expensive algorithm due to longer convergence time
Dropouts	Skips connections between layers by creating holes; avoids overfitting; causes increased number of iterations for convergence
Batch normalization	Batch-wise normalization of input data to increase the stability network architecture; results in faster training and higher learning rate; causes computational overhead during training
<b>Deep learning strategies</b>	
Supervised learning	Learning from a labeled dataset; most popular examples are CNNs; provides greater accuracy and efficiency in various medical imaging tasks
Semi-supervised learning	Used when only a part of the training data is labeled; learning from a small number of labeled examples and a large number of unlabeled examples; can utilize a pretrained network
Unsupervised learning	Learning from completely unlabeled data where the model learns to make decisions based on similarity and structure on its own
Reinforcement learning	Learning by interacting with the environment for sequential decision making; in deep reinforcement learning, neural networks approximate one or more components of reinforcement learning; nonlinear function approximation may face instability and divergence
Transfer learning	Learning from a model trained on another dataset is transferred to a new problem; provides rapid progress in the training of new problem; works with similar problems only
<b>Popular architectures</b>	
AlexNet <sup>16</sup>	One of the first high performance architecture; notable features include use of ReLUs, dropouts, split computations on graphic processing units, and data augmentation
VGG <sup>107</sup>	Popularized the idea of using several deeper layers for training and using smaller filter kernels
ResNet <sup>108</sup>	Introduced skip connections in a 152-layer network that made the network learns residuals and fine details
GoogLeNet <sup>109</sup>	Contained multiple inception modules, where multiple filters of different sizes are applied to inputs and their results concatenated; also popularized not using fully connected layers, and thus, reducing the number of training parameters
DenseNet <sup>110</sup>	Well suited for smaller datasets; works on feature reuse and lowers the model parameters at a given depth
YOLO <sup>111</sup>	Fast and simplified network to perform object classification and segmentation; pretrains a simpler version of the network and can enable real-time processing with reasonable predictions
GANs <sup>112</sup>	Generative adversarial networks have two networks, one that creates samples and the other that classifies them; useful in image synthesis
Siamese nets <sup>113</sup>	Contains two identical networks and shares same weights between two different inputs; used to find similarity between inputs by comparing feature vectors; needs more training time than normal networks and is slower
U-Net <sup>80</sup>	A very successful network in biomedical image segmentation tasks; network has two parts, first part downsamples the images and second part upsamples them; can create high resolution results
V-Net <sup>114</sup>	A 3D version of U-Net with volumetric connections and skip connections

Abbreviations: CNN, convolutional neural network; GAN, generative adversarial network.

### 3.6 | Common problems and solution strategies in deep networks training

One of the major factors that determine success in deep learning performance is the availability of a large labeled dataset. However, in the field of medical imaging in general and in ultrasound elastography in particular, this requirement has been difficult to meet. Several reasons include the requirement of a clinical expert in this specialized field, associated high costs, ethical, legal, and governmental legislation issues, and having a small dataset for some diseases that are not so common. Most medical imaging studies struggle to recruit more than

1000 patients for data collection, whereas deep learning applications in computer vision or robotics may include well beyond one million labeled images. Therefore, having to train a deep neural network with limited training data is a challenge.

In addition, small datasets also suffer from the class imbalance problem, that is, the number of samples in one class being not comparable to another class. It is known that an imbalance in the training set may reduce the accuracy of the ANN. Practically, this means that when collecting medical images, the number of normal/healthy image results may be considerably more than those with abnormal/unhealthy results, or vice

versa in the case of very malignant conditions. Many techniques are available to deal with this challenge, one can be to undersample (i.e., reduce the amount of the majority class group), to oversample (i.e., duplicate some samples of the minority class), or combine these two approaches. Data augmentation is also an effective weapon to combat the problem: One can artificially generate more samples without actually collecting new data. The most commonly used methods include cropping/padding, blurring, and rotating parts of the existing images. Alternatively, one may also attempt to assign different weights to the cost function of different classes, so as to compensate for the imbalance issue, that is, make it more costly when a minority sample is misclassified. Although image transformation is a common approach for data augmentation, an undercovered challenge in ultrasound imaging and especially ultrasound elastography is to consider the physics of wave propagation to better represent artifacts in image formation (e.g., wave attenuation, wave reverberation, and wave diffraction impacting the quality of clinical images), and nonrigid motions.

The training of CNNs is monitored with an error function on training and output data. The errors are back-propagated to CNNs to adjust inner parameters and reduce the error. Different optimizers are used to adjust parameters within CNNs, such as stochastic gradient descent, AdaGrad, and Adam optimizers. The learning of a model can be iterated with single input data, groups of input data, or all the input data. However, minibatch learning is more popular than batch learning to make the model computationally efficient. Minibatch learning usually demands data shuffling during each epoch. A higher number of epochs usually result in better performance, but it is not necessary because sometime a network can learn too much and cause overfitting. Overfitting may also commonly arise due to training with limited data. To avoid overfitting, several strategies have been developed that include well-designed initialization,<sup>115</sup> stochastic gradient descent optimization,<sup>116</sup> efficient activation functions,<sup>117,118</sup> dropouts,<sup>119</sup> and other powerful intermediate regularization methods.<sup>120</sup>

A useful strategy for training an end-to-end deep learning model is to use nonlinear activation functions due to the large dynamic range and modulated nature of RF ultrasound channel data. The ReLUs that are otherwise popular in computer vision tasks, due to their positive unbounded output, cause many dying nodes for ultrasound channel data due to the presence of abundant negative values. Instead of ReLUs, either hyperbolic tangent functions or a class of concatenated ReLUs that preserve both positive and negative values could be used to overcome this issue.<sup>121</sup> It is also important to consider the potential impact of subsequent signal transformations in the deep learning processing chain as RF ultrasound signals may undergo considerable dynamic range compression. This could be due to

logarithmic transformations to project the large dynamic range of the channel data onto the limited range of a display. A mean square logarithmic error can be incorporated in the deep network's training loss to compensate for the issue of dynamic range.<sup>20</sup>

In the context of image reconstruction, model-based methods have traditionally been popular in medical imaging due to their reliability. New methods that utilize models and structure together with learning from data can perform extremely well even with limited training datasets. For example, model-based image reconstruction requires finding an optimal regularization, whereas an end-to-end deep learning model can reconstruct images directly from raw data. Instead of performing an end-to-end task, a deep learning model can be trained to perform optimal regularization, and a model-based algorithm can be utilized to reconstruct images. This could improve image quality by learning structures through the deep network and increase reliability in reconstruction by employing a model-based algorithm. Aggarwal et al. proposed a framework called MoDL (model-based reconstruction using deep learning priors) that combines model-based frameworks with a deep learning model.<sup>122</sup> They have proposed a variational framework that involves a data consistency term and a learned CNN together to capture the image redundancy. The data consistency term is a quadratic subproblem that may be solved either analytically for simpler problems or through an optimization solver, such as a conjugate gradient for complex problems. In this framework, a low complexity plug-and-play CNN with a considerably low number of parameters is sufficient to learn the image set.<sup>122</sup> This latter approach remains to be tested with ultrasound elastography datasets.

The neural network's ability to process clinical images with deep down- and upsampling (e.g., U-Net) can be useful in improving image quality and perform efficient image segmentation.<sup>123</sup> The end-to-end deep networks can be immensely useful in avoiding intermediate data/image processing steps.<sup>124</sup> Deep learning methods have shown their advantages not only in improvement in image quality but also in fast imaging computations. For example, transfer learning from different medical modalities or organs can be adopted in ultrasound elastography without having access to large datasets.<sup>82,125,126</sup> GANs have the ability to create synthetic datasets that can be utilized for data augmentation to alleviate the data scarcity.<sup>127,128</sup>

The advanced data-driven learning capability of deep learning models makes them a promising candidate to tackle the challenge of the inverse problem in elasticity by targeting high-dimensional nonlinear mapping. From the data generation (for training) point of view, the generation of a tissue deformation field can be done by simulating a suitable elasticity distribution and solving the forward problem of wave propagation, which is relatively easy to compute. For example, finite elements

method can be used to estimate the deformation fields of a given elastic tissue model with sufficient precision.<sup>73</sup> This data can then be utilized to train the model with a high-dimensional mapping between the ground truth and the wave field images. Thus, inverse problem in tissue elasticity can be handled in a data-driven way and probably by avoiding the challenge of noisy data and ill-posedness for various inverse problems.<sup>129</sup> As an example, a conditional GAN was proposed recently,<sup>73</sup> where the generator aimed at creating suitable elasticity images of the tissue model, whereas the discriminator aimed at identifying fake elasticity images created by the generator from the real ones. The training continued until Nash equilibrium is reached, that is, the generator creates modulus images so real that the discriminator cannot differentiate them from the ground truth. In addition, minimization of the  $L_1$  and  $L_2$  losses of the prediction is also involved in the training procedure for better performance. The model was able to achieve an accuracy of over 99%.<sup>73</sup>

## 4 | DEEP LEARNING APPLICATIONS IN ULTRASOUND ELASTOGRAPHY

### 4.1 | Quasi-static elastography applications

In the last 5 years or so, deep learning has encouraged the development of new quasi-static elastography algorithms. For motion estimation problems, deep learning was originally applied to OF estimations in computer vision, in which a CNN-based architecture was constructed to perform end-to-end OF estimation without feature extractions, as shown in Figure 5. The first network called FlowNet<sup>130</sup> was proposed in 2015, which demonstrated competitive accuracy with conventional state-of-the-art OF algorithms, but with higher computation efficiency. Following it, other CNN-based networks were developed, such as FlowNet 2.0,<sup>131</sup> SpyNet,<sup>132</sup> LiteFlowNet,<sup>133</sup> and PWC-Net,<sup>134</sup> to achieve better accuracy. To our knowledge, the first two contributions that utilized CNN-based OF architecture for ultrasound quasi-static elastography were published in 2018. One used a retrained FlowNet 2.0 with an additional ultrasound dataset to estimate breast strains.<sup>88</sup> This is the first feasibility study of deep learning in quasi-static ultrasound elastography. Although the obtained strain image quality was lower than that using the cross-correlation method, the additional training dataset from simulated ultrasound RF signals was proven to be beneficial for accuracy improvement. The other study utilized FlowNet 2.0 directly to get a coarse estimate, and then the initial displacements were refined using a global ultrasound elastography method, named Global Ultrasound Elastography Network.<sup>135</sup> The strategy of an initial estimation with FlowNet and fine-tuning with a

conventional displacement estimation method showed robustness against decorrelation noise induced by large inter-frame motions. Recently, the same group proposed an RF Modified PWC-Net (RFMPWC-Net) to obtain similar performance as state-of-the-art conventional elastography methods for liver strain imaging but outperformed FlowNet 2.0 and original PWC-Net.<sup>136</sup> Other than five pyramid levels of PWC-Net, the final pyramid level of the RFMPWC-Net also included the features extracted from RF data for accurate displacement estimations. A total variation regularization regarding displacement gradients was added into the new cost function to reduce displacement variations. With pretrained weights of the original PWC-Net, the additional 1000 image pairs of simulated displacements were used to fine-tune the proposed network, which improved the performance of displacement estimations. A thorough evaluation of CNN-based OF networks for breast ultrasound strain elastography can be found in Ref. [137].

The straightforward translation from CNN-based OF architectures in computer vision to ultrasound quasi-static elastography is not adequate for accurate strain estimations. The main reason is that previous CNN-based networks were trained by datasets of photographs in which only rigid motions were represented.<sup>137</sup> However, tissue motions are more complex, including both rigid displacements and non-rigid deformations and rotations. In addition, previous studies only utilized deep learning architectures to estimate displacements. An additional gradient operation is performed to derive strains. Thus, other CNN-based networks, which are trained with ultrasound simulation datasets based on biomechanical models and ultrasound physics-based reconstructions, have recently been proposed to provide end-to-end direct strain estimations. Wu et al. exploited two cascaded CNNs to reconstruct strains directly from RF signals.<sup>124</sup> The two-stage processes, that is, RF signals-to-displacements and displacements-to-strains, were respectively replaced by two separated CNNs, and the two networks were trained simultaneously using 40 image pairs of displacement and strain fields. The test results on 42 phantom data and 4 patient data indicated that the model could predict strain maps with higher signal-to-noise and contrast-to-noise ratios than a classical state-of-the-art method. A recent work of an end-to-end strain network is shown in Figure 6, which incorporated two cascade subnetworks.<sup>138</sup> Displacements and strains were first computed by biomechanics simulations using a finite elements analysis. The causal relationship among RF signals, displacements, and strains, namely, RF signals causing displacements and displacements causing strains, enabled displacements to be privileged information to be added into the intermediate layer between the two subnetworks. The privileged information was able to provide the extra supervision

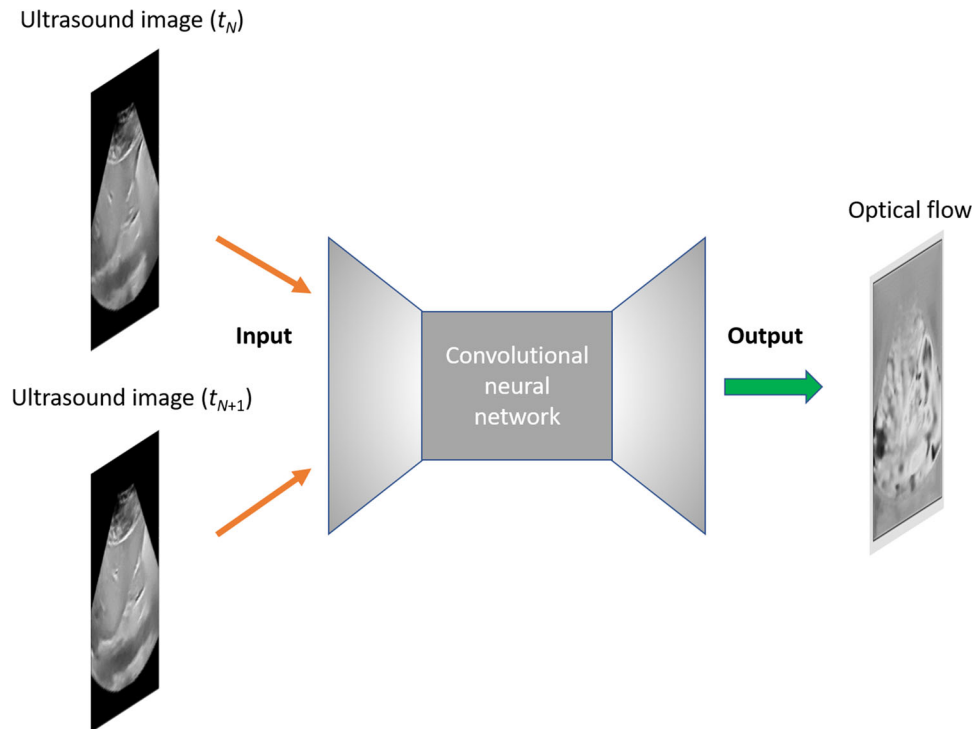


**FIGURE 5** Architecture based on a neural network that learns to estimate end-to-end optical flow tracking of motions from ultrasound images. The input is a pair of ultrasound images and the outputs are optical flow estimations.

information to guide the network training. The network was trained with a part-to-whole procedure, using 100 image pairs of displacement and strain fields. Specifically, the two subnetworks were trained separately using different loss functions in terms of displacement and strain values, respectively. Then, the entire network was trained with the combined loss function. This learning-using-privileged-information paradigm corrects the intermediate state of the learning process,<sup>138</sup> which allows the network to outperform state-of-the-art methods in terms of effectiveness and efficiency.

For myocardial elastography, FlowNet 2.0 was also incorporated to automatically assess myocardial function of the left ventricle in 2D echocardiography.<sup>139</sup> The model was trained with three public synthetic datasets widely used for training and evaluation of OF methods in computer vision. Then, the trained model was evaluated on 21 subjects with cardiac diseases, whose performance was compared to the elastography method implemented on the commercial ultrasound system used. The average global longitudinal strains with the deep learning method ( $-17.3\% \pm 2.5\%$ ) was in good agreement with the commercial method ( $-17.9\% \pm 2.3\%$ ). More recently, the same group proposed EchoPWC-Net for automated myocardial function imaging,<sup>140</sup> which is a modified PWC-Net removing the feature warping at each level. Other than synthetic datasets mentioned before, a simulated cardiac ultrasound dataset<sup>141</sup> was used for training, which included

6165 images with known displacements. In addition to basic data augmentation, four common artifacts in echocardiography were induced as specific ultrasound augmentation schemes, namely, acoustic shadow, acoustic haze, depth attenuation, and speckle reduction, to increase the robustness of the model. The evaluation test of global longitudinal strains on 30 patients showed a significant correlation with a commercial method with a correlation coefficient of 0.96, although with an underestimation of large strains due to predominant small strains in the training dataset.

As robust motion estimation is difficult for a left ventricle because of large translations, rotations and strains, and out-of-plane motions, some biomechanical prior assumptions, such as spatiotemporal smoothness, are explicitly embedded in motion-tracking methods to regularize motion fields and alleviate unreliable motion estimations. Lu et al.<sup>142</sup> proposed to use a multilayered perceptron network that was trained with a synthetic cardiac dataset to learn a latent representation of spatiotemporal regularization. The neural network-based spatiotemporal regularization coupled with a motion-tracking method showed improvement in tracking performance compared with no regularization. A more recent work extended the multilayered perceptron network to include biomechanical constraints.<sup>143</sup> Incompressibility and periodic motion of cardiac tissues were introduced into the cost function. The biomechanically inspired constraints alleviated the poor tracking

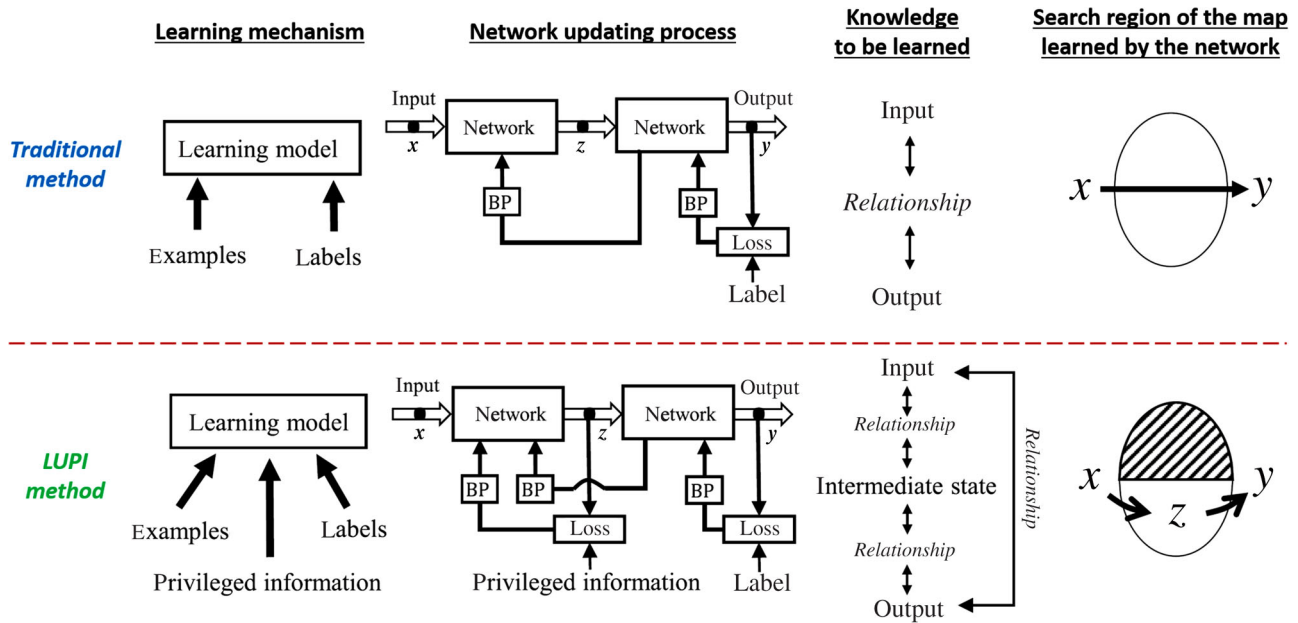


**FIGURE 6** Overview of classic neural network methods and the learning-using-privileged-information (LUPI) network. Traditional methods learn to predict input  $y$  from input  $x$  using labeled data. The LUPI network added privileged information into a loss function to provide an extra supervision information, which guided directly the inner feature representation and helped correct the intermediate state in the learning process. BP, back propagation. *Source:* Adapted with permission from Ref. [138].

performance of the trained model, by using a synthetic dataset adapted to an in vivo dataset. This work showed the capability of identifying infarcted cardiac regions in a canine model, which was verified by manually traced infarcted regions from postmortem excised hearts.<sup>143</sup>

## 4.2 | Dynamic elastography applications

The development of deep neural networks in dynamic elastography has resulted in several clinical applications detailed next, which include a classification of breast tumors,<sup>144,145</sup> liver imaging,<sup>146–148</sup> thyroid nodules imaging,<sup>149</sup> elastography of plantar fasciitis,<sup>150</sup> and prostate cancer.<sup>151</sup> Such studies have been in the recent trends of the last decade. Architectures based on CNNs remain the most popular choices, whereas most studies have focused on either the classification of benign and malignant tumors, or on estimating the tissue stiffness. Let us review these studies while categorizing them according to their application.

### 4.2.1 | Applications in breast tumor classification

SWE is being widely used for cancer screening, especially in breast cancer research. In general, malignant breast tissues are stiffer than healthy/benign ones, and morphological data can provide important clinical information. Ultrasound B-mode features have been widely used in conjunction with dynamic elastography data

for breast tumor classification, and the breast imaging reporting and data system has standardized the use of these approaches for diagnosis.

An SWE study based on a deep belief network of two-layer architecture comprising a point-wise Boltzmann machine and a restricted Boltzmann machine showed that deep learning features could achieve higher classification performance than conventional machine learning approaches with 93.4% accuracy, 88.6% sensitivity, and 97.1% specificity.<sup>144</sup> The continued development of deep learning showed great potential for classification, especially by utilizing CNN architecture. A CNN-based radiomics classification model for SWE data was first implemented by Zhou et al.<sup>152</sup> The developed network could automatically extract a large number of features from the recorded dataset, including small structures/edges, as well as high level high-abstraction information. Their model reported as much as 4224 features extracted by the whole CNN architecture.<sup>152</sup> The first several layers of the CNN learned low-level features that have small receptive fields such as edges and corners. The middle layers learned to detect a part of the tumors. The top layers had larger receptive fields and could learn high-level, high-abstraction, and semantic features, such as parts and objects. The only manual intervention required when using such architecture was selecting the ROI, which was done by experienced radiologists. There was no requirement for segmentation algorithms to extract crafted features such as contours, sizes, or shapes. Figure 7 shows a schematic diagram of the CNN architecture that was used in the latter study for tumor classification.

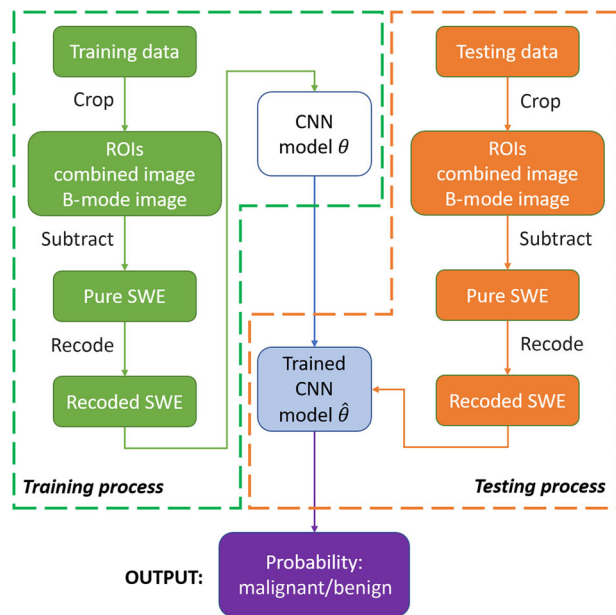


**FIGURE 7** Schematic diagram of convolutional neural network (CNN) for the classification of breast tumors on recoded shear wave elastography (SWE) images. *Source:* Adapted with permission from Ref. [152].

Often in deep learning based studies, ultrasound elastography is utilized as a supporting parameter to other clinical ultrasound images to quantify a tumor grade by using a standardized color scheme. Combining elastography with B-mode ultrasound imaging is probably more useful than combining color Doppler with B-mode ultrasound for differentiating small, oval, or round triple-negative breast cancers from fibroadenomas. Yeo et al. reported this conclusion after analyzing data from 68 fibroadenomas and 63 triple-negative breast cancers smaller than 2 cm.<sup>153</sup> The average area under the receiver operating curve (ROC) for B-mode with elastography was 0.869, which was significantly higher compared to B-mode with color Doppler imaging that was 0.576. A deep polynomial network AI architecture for the automated extraction of dual-modal image features from both SWE and B-mode ultrasound, with the leave-one-out cross-validation, resulted in a sensitivity of 97.8%, a specificity of 94.1%, and an accuracy of 95.6%.<sup>145</sup> The performance of classification between benign and malignant breast tumors was better than single-modal using either B-mode ultrasound or SWE. Machine learning architectures based on support vector machines have also utilized tissue elasticity data for breast tumor segmentation. A novel system that could obtain quantitative elastographic information from color SSI elastography images was proposed to classify benign and malignant breast tumors based on a dataset of 125 lesions from 93 patients.<sup>154</sup> A support vector machine classifier was used and 90.9% sensitivity and 97.5% specificity were achieved.

Compared to other imaging modalities such as X-ray mammography or magnetic resonance imaging, AI architecture has been utilized less often in the ultrasound field in general and ultrasound elastography in particular. One of the main reasons is that poor image quality is observed when a large amount of tissues is examined by the ultrasound field, and shadowing of tumors makes their contours unclear. Also, in SWE, images can be misinterpreted if the probe is pressed harder.<sup>51</sup> Difficulty in data collection and recruiting a large number of patients, as mentioned earlier, are other reasons for fewer publications. The role of data augmentation, shown to be useful in avoiding overfitting and improving classification performance in various fields, has not been explored much in these studies on elastography and remains a low hanging fruit.

#### 4.2.2 | Applications in liver imaging

Chronic liver disease is a major health problem with most prevalently including nonalcoholic fatty liver disease and viral hepatitis. Liver biopsy remains the common method for diagnosis, which is an invasive histologic reference standard with risk of complications. The liver imaging reporting and data system is the standardized classification system for imaging liver lesions and related diagnosis. Elastography for the assessment of liver stiffness has replaced the need for a great majority of liver biopsies. However, an unequivocal advocacy of elastography as a complete replacement for a liver biopsy is still not established, and challenges in obtaining a perfect assessment of full-bodied patients with large body mass indexes, steatosis, or very stiff livers still need to be overcome.<sup>37,50,155</sup> Recent developments include deep networks that estimate liver fibrosis severity from ultrasound texture,<sup>156</sup> deep learning radiomics of SWE images,<sup>147</sup> and the continued study of AI-based methods for medical imaging of the liver.<sup>146,148</sup> Treacher et al.<sup>156</sup> collected gray-scale elastography images from 326 patients, including 3500 images with corresponding SW velocity measurements. The study used this data to train and validate 100 different CNN architectures. The study concluded that there was no substantive association between gray-scale elastography texture and SW velocity.

Future objectives for the development of elastography systems include the diagnosis of inflammation, an important factor in the pathogenesis of nonalcoholic steatosis (NASH) or viral hepatitis. A deeper understanding of the significance of the tissue mechanical properties as a standalone predictor of clinical outcomes is also desired. Elastography will continue to have rapid developments in the near future and AI-based diagnostic methods may have the potential to completely overturn the challenges faced in current state-of-the-art ultrasound B-mode and elastography

imaging standards. In fact, deep learning methods based on ultrasound imaging data have shown accuracy up to 100% in detecting fatty liver disease and making risk stratification.<sup>146,147,156,157</sup> A study conducted among 398 patients for the staging of liver fibrosis (grades F0–F4) using SWE and a CNN model achieved area under the ROC curve (AUC) values of 0.97 for F4, 0.98 for >F3, and 0.85 for >F2.<sup>147</sup> AI studies in ultrasound B-mode liver imaging as well as in elastography have accelerated in recent years, consistently achieving sensitivity up to 100% and accuracy in the range of 97%–100% with either support vector machine or CNN-based models.<sup>158–161</sup> Of course, further validations with extensive datasets are still required to confirm those performances.

One of the first AI models was a machine learning study based on a support vector machine model and a computer-aided diagnosis system for the classification of chronic liver disease using 2D-SWE imaging.<sup>162</sup> This study included a dataset of 126 subjects, and a stiffness value clustering algorithm was employed to extract 35 features indicative of physical characteristics within SWE images. The study reported an accuracy of 87.3% with sensitivity and specificity values of 93.5% and 81.2%, respectively.<sup>162</sup> Wei et al.<sup>163</sup> proposed to reconstruct a clinical scoring system for an improved detection of advanced hepatic fibrosis and cirrhosis in hepatitis B and C virus patients. The analyses were performed using three machine learning methods, namely, decision trees, random forests, and gradient boosting methods on 576 hepatitis B and 484 hepatitis C patient datasets. The study also developed a publicly accessible web-tool, LiveBoost, to use in clinical practices. Recently, deep models have become a more popular choice due to their better performance, as summarized next.

A multicenter study named deep learning radiomics of elastography (DLRE) was conducted by Wang et al.<sup>147</sup> to assess liver fibrosis stages on 398 patients from 12 hospitals with 1990 2D-SWE images. The patients had chronic hepatitis B, and histology obtained from liver biopsy was used as a reference. They reported an AUC for a cirrhosis of 0.97, for an advanced fibrosis of 0.98, and for a significant fibrosis of 0.85 with the use of the DLRE architecture. A schematic of the DLRE architecture is shown in Figure 8. Another study aimed at assessing chronic liver disease with multiple deep learning networks, including GoLeNet, AlexNet, VGG16, testNet50, and DenseNet201, utilized SWE images acquired from 200 patients and registered an accuracy ranging from 87.2% to 97.4%, which outperformed the radiologists' performance at least by 10%.<sup>164</sup> Treacher et al.<sup>156</sup> focused on studying the texture pattern in gray-scale elastography images to estimate SW velocity in liver fibrosis patients and investigated a total of 100 CNN architectures. Brattain et al. developed an automatic framework to classify liver fibrosis stages using SW elastograms.<sup>165</sup> The CNN-based classifier

provided an AUC of 0.80 versus 0.69 using a reference manual approach. Multimodal ultrasound imaging combining B-mode images with SW elastograms achieved a better grading of liver fibrosis than B-mode or SWE alone.<sup>126</sup> Another work studied the prediction of hepatocellular carcinoma occurrence using a combined CNN and support vector machine model.<sup>166</sup> It showed a predictive accuracy of 90%, when considering B-mode images, SW elastograms, sex, and age. Gatos et al.<sup>167</sup> performed a study to automatically detect and isolate areas of low and high stiffness temporal stability in SWE images to define their impact in chronic liver disease diagnosis.

Deep learning studies for liver imaging face the challenge that the acquired dataset is not of superior quality, often due to ultrasound attenuation in large body size. In addition, differences in imaging systems could affect the image display. Moreover, the imaging acquisition and examination need to be unified among operators to construct a well-qualified imaging database. The implementation of transfer learning strategies and further deep learning advancements could improve classification accuracy.

#### 4.2.3 | Applications in thyroid nodule classification

Thyroid nodules are abnormal lumps in the organ, which may be indicators of cancer. As for other organs, the standardized diagnostic algorithm for TI-RADS provides a score to indicate the risk of malignancy of the thyroid gland. Confirmation of diagnosis still requires fine needle aspiration biopsy; however, due to its complexity, about 10%–20% of thyroid nodule biopsies tend to be nondiagnostic.<sup>168</sup> Qin et al.<sup>149</sup> utilized a combined B-mode and elasticity image dataset as an input to a CNN architecture for combining depth features of these images to form a hybrid space for the classification of benign and malignant thyroid nodules. The CNN was pretrained on an ImageNet database and a transfer learning strategy was used to extract image depth features in ultrasound images. Depth features of B-mode and elasticity images were combined to form a hybrid feature space, and an end-to-end CNN model was implemented. The study used 1156 thyroid nodule images in 233 patients and reported an accuracy of 94.7%. Several other deep learning studies utilized only B-mode ultrasound images for thyroid nodules classification, including Ma et al.<sup>169</sup> who fused two CNNs pretrained on an ImageNet database to achieve higher accuracy; Peng et al.<sup>170</sup> who created a network called ThyNet trained on 18049 images from 8339 patients and tested on 4305 images of 2775 patients to achieve an accuracy of 92.2%; and Zhou et al.<sup>171</sup> who performed deep learning radiomics of thyroid ultrasound images based on a transfer learning strategy with a dataset of

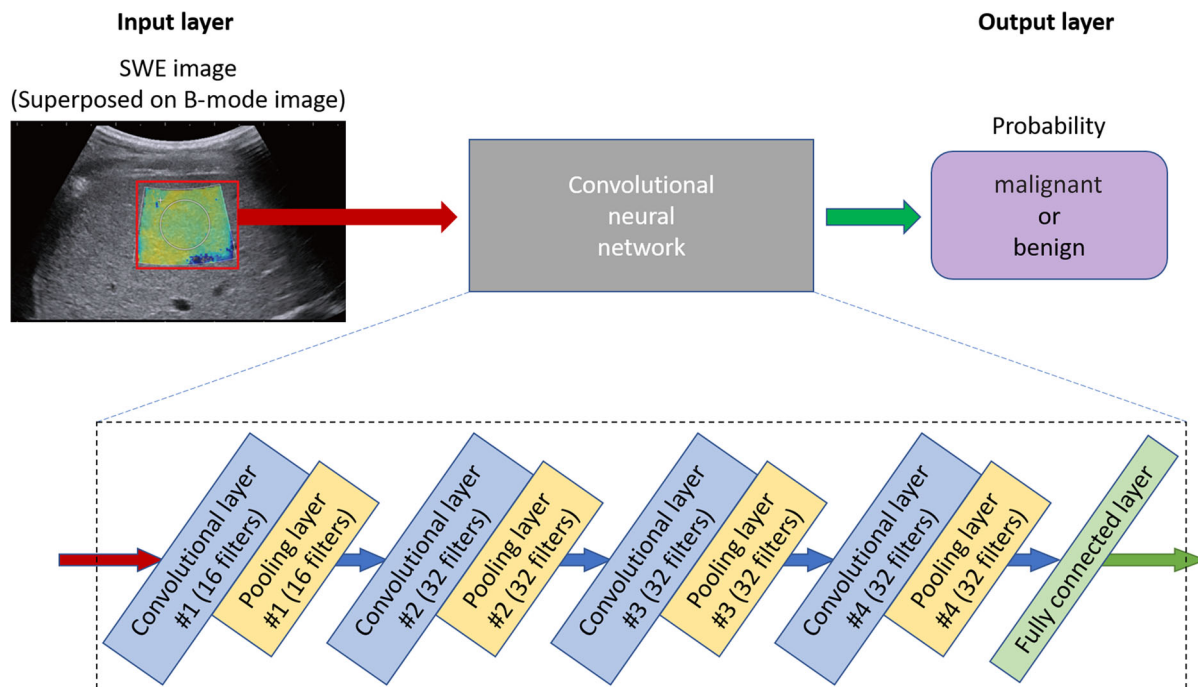


**FIGURE 8** Illustration of the deep learning radiomics in elastography (DLRE) architecture that takes a two-dimensional (2D) shear wave elastography (SWE) image as inputs to predict liver fibrosis stages. The input layer follows a four convolution-pooling procedure (C1-P1 to C4-P4), and the last pooled maps are fully connected with 32 neural nodes that perform classification. *Source:* Adapted with permission from Ref. [147].

1750 thyroid nodule images and achieved an AUC score of 0.96. As far as we are aware of, no other deep learning studies based on ultrasound elastography images have been reported, and the field remains open for further exploration.

#### 4.2.4 | Other clinical applications

In addition to the three main applications discussed here, AI-based diagnostic research is being carried out for several other clinical applications. One of the first such applications was in endoscopic ultrasound elastography for the diagnosis of focal pancreatic masses with a data size of 778 recordings from 258 patients, where multilayered perceptron architecture was used.<sup>172</sup> The neural network model had two hidden layers and was trained with the backpropagation algorithm that achieved 84.27% in testing accuracy. In 2D-SWE, Gao et al.<sup>150</sup> developed a deep Siamese framework with multitask learning (DS-MLTL) and transfer learning, which could learn discriminative visual features and effective recognition functions for the classification of plantar fasciitis, a common cause of heel pain. The study also reported that their network resulted in higher sensitivity (78.3%) and specificity (91.7%) compared to other popular deep learning methods, namely, the CNN model (sensitivity = 75.0%, specificity = 86.7%), transfer learning model (sensitivity = 71.7%, specificity = 88.3%), and DS-MLTL model

(sensitivity = 76.7%, specificity = 86.7%). Table 3 provides a summary of technical informations on different clinical applications. As seen, various AI models were used and training, and test sets were limited with less than 1500 images acquired from less than 700 patients.

#### 4.2.5 | Limitations being resolved by deep learning technologies

It is worth mentioning that AI architectures have also been utilized in several system development-related applications that could be used in elastography, such as beamforming<sup>175</sup> and inverse problem solution in elasticity imaging.<sup>129</sup> Patel et al.<sup>129</sup> developed a CNN model that accepted measured displacements as inputs and trained it to classify tumors based on their heterogeneity and nonlinearity. A 5-layered CNN was utilized for training 8000 synthetic samples of tissue heterogeneity, and a 4-layered CNN was utilized for training 4000 synthetic samples of nonlinear elasticity, and accuracies of 99.7%–99.9% were reported. The model was also validated on data obtained from 10 patients with breast lesions. The scope for both deep learning-based advanced architectures seems to be endless in medical diagnostics. It is expected that elastography data in combination with conventional ultrasound data could greatly improve the diagnostic accuracy, and advantages are manifold. Rightly so, deep learning has been dubbed as a paradigm shift in medical imaging<sup>176</sup> that

**TABLE 3** A summary of clinical diagnostic applications using dynamic elastography and deep learning methods

Disease/application	AI classifier	Training dataset (images)	Testing dataset (images)	Accuracy (%)	Sensitivity/ Specificity (%)
Breast tumors <sup>145</sup>	Deep polynomial network	227 dual mode (SWE and B-mode ultrasound) from 121 patients		95.6	97.8/94.1
Breast tumors <sup>152</sup>	CNN	400 (training) and 140 (testing) from 205 patients		95.8	96.2/95.7
Breast tumors <sup>173</sup>	Multiple CNNs	304 (training) and 73 (testing)		0.87 (AUC)	85.7/78.9
Breast tumors <sup>174</sup>	Multiple CNNs	584 breast lesions		85.7	79.1/93.6
Breast tumors <sup>144</sup>	Unified point-wise gated Boltzmann machine-based two-layer deep learning architecture	227	5	93.4	88.6/97.1
Chronic liver disease <sup>164</sup>	CNN	140	60	87.2-97.4	–
Liver fibrosis <sup>165</sup>	CNN	515 patients	103 patients	0.80 (AUC)	–
Liver fibrosis <sup>126</sup>	CNN	364 patients	102 patients	0.95 (AUC)	90.1/94.3
Hepatocellular carcinoma <sup>166</sup>	CNN	1302 from 262 patients	434 from 86 patients	0.90 (AUC)	83.3/96.3
Hepatitis B virus-associated fibrosis <sup>147</sup>	CNN	1330 from 266 patients	660 from 132 patients	0.98 (AUC)	90.4/98.3
Liver fibrosis <sup>167</sup>	CNN	200 from 200 patients		82.5-95.5	–
Thyroid nodule <sup>149</sup>	CNN	908 from 183 patients	248 from 40 patients	94.7	92.7/97.9
Plantar fasciitis <sup>150</sup>	Deep Siamese framework	720	360	85.0	76.8/93.3

Abbreviations: AI, artificial intelligence; AUC: area under the receiver–operating curve; CNN, convolutional neural network; ReLU, rectified linear unit; SWE: shear wave elastography.

could achieve optimal results cost-effectively, especially from large and compromised datasets, as well as for nonlinear, non-convex, and overly complex problems.

Deep learning-based models have been very useful in tasks that require a dense output, such as voxel classification in 3D image segmentation.<sup>177</sup> This has reduced the labor and cost of manually annotating tissue boundaries, bones, etc. In addition, deep learning has been useful in assisting radiologists and other clinicians in decision-making by improving image quality. End-to-end deep learning models, which avoid multi-stage dependency from one stage to the next, have the potential to provide new dimensions in computer-aided diagnosis by combining computer vision with medical imaging.<sup>178</sup> However, proposing end-to-end models for accurate lesion recognition still remains challenging due to unavailability of large datasets for training. Image-to-image translation, where images of one modality can be transformed to images of a different modality, is a new domain made possible by deep learning models. Models such as pix2pix network use conditional GANs for image-to-image translation with pixel-to-pixel correspondence,<sup>179</sup> whereas cycleGAN can be applied to unmatched images and does not require pixel-to-pixel correspondence.<sup>91</sup> Another domain is super resolution where deep learning has performed well in medical imaging applications due to the network's deep layers'

ability to up-sample the images efficiently and accurately. Many super resolution models such as FUS-Net are based on extensive down- and up-sampling of the images.<sup>123,180</sup> GANs have been used for super resolution in ultrasound elastography.<sup>181</sup> Deep learning methods also have the ability to create synthetic elastography images from ultrasound B-mode images.<sup>83</sup> Image fusion is another feature of deep learning, which is a future scope in ultrasound elastography by now, but is already popular for other imaging modalities.<sup>182,183</sup>

## 5 | CONCLUSIONS AND PERSPECTIVES

Deep neural networks provide automated solutions for several clinical problems that may require expert skills for humans. There are two major fields of clinical AI research: (1) image processing/analysis that involves denoising, feature extraction from images, segmentation, etc., and (2) image formation/reconstruction, that is, from data to images. Even though a deep network is fundamentally different from multi-resolution analysis or optimization models, the major virtue of deep networks is the nonlinear learning and non-convex optimization ability. However, the lack of curated training data is a major limitation in advancing any AI

model. Clinical translation of fully automated deep learning models for diagnosis tasks may take a few years as it would require absolute confidence by the clinical community. There is a need to develop more advanced algorithms to solve more complex medical problems, especially in ultrasound imaging. There is also a need to validate diagnostic assistance methods (e.g., heatmaps<sup>184</sup>) providing feedback to clinicians instead of final diagnosis.

This article summarized several studies that implemented deep learning methodologies for ultrasound elastography applications, particularly for image analysis and feature extraction. In the next paragraphs, a discussion is given on some prospective topics of research that have not yet been explored much in ultrasound elastography AI research.

There has been relatively limited research conducted on image reconstruction in SWE applications, which remains a low hanging fruit.<sup>185</sup> Deep learning-based reconstruction algorithms have data-driven knowledge-enhancing abilities that provide smarter initial guess, more relevant features extraction, and application-specific regularized final images. If a dataset is severely compromised due to truncation, distortion, noise, or artifacts, a model-based iterative or analytical algorithm can be used for initial reconstruction and subsequently used as an input to deep network.<sup>186</sup> This two-step process for image reconstruction can be extremely useful in elastography applications. Such networks can become favorable as deep networks with images as inputs can easily be adapted and domain-specific data can be incorporated as unprecedented prior knowledge. Bandwidth enhancement of recorded data is another open field<sup>187</sup> that can improve reconstruction algorithms in ultrasound elastography.

Nonuniform approaches to acquire data in SWE are a major challenge that restricts the unification of various databases. Recently, efforts have been made to address this by creating unifying standards and a list of recommendations for data acquisition. The Radiological Society of North America's Quantitative Imaging Biomarkers Alliance was one of the first initiatives toward unifying standards for identifying needs, barriers, and solutions in clinical imaging by uniting researchers, health-care professionals, and the industry.<sup>188,189</sup> The World Federation for Ultrasound in Medicine and Biology published a set of guidelines in 2017 for clinical use of elastography.<sup>190</sup> The European Federation of Societies for Ultrasound in Medicine and Biology's publications are a further extension to this list where an extensive set of recommendations are made on data acquisition for use in liver ultrasound elastography.<sup>191</sup> Researchers and industry professionals in the field are encouraged to follow these recommendations for SWE data acquisition so that a larger unified database can be established, which would be immensely useful in developing deep learning models in ultrasound SWE.

The network design remains a popular topic of research in terms of both overall architecture and component characteristics.<sup>80,144,145,192</sup> This is equivalent to algorithmic design or computer architecture design, which still is a prominent topic for specific applications such as elastography. Another important field is unsupervised learning that has been explored in magnetic resonance and computed tomography imaging modalities for tasks such as denoising,<sup>193</sup> motion correction,<sup>194</sup> and synthetic image generation using GAN<sup>195–197</sup>; similar exploration is needed in ultrasound elastography applications. A futuristic hope is that deep neural networks can be further advanced by mimicking neuroplasticity of the brain—the ability to form new connections, update how nodes are connected, and reorganize itself for improved learning and adaptation.<sup>176,198</sup>

As mentioned a few times in this review, one of the main challenges in deep learning applied to medical imaging is the unavailability of large datasets. If the scarcity is only related to the labeling of the data, semi-supervised learning and data augmentation approaches could help. Many tasks require predictions to be insensitive to certain variations in data. Classical intensity augmentations such as histogram manipulation, addition of noise, augmentation (e.g., scaling, cropping, flipping, padding), rotation of images, etc. can be utilized to increase the dataset size. However, to be more specific to challenges relevant to the field of ultrasound imaging, considering data augmentation using image transformations based on acoustic physics concepts may be privileged to better mimic clinical variabilities. Another strategy to use the limited data is to train the network efficiently. CNN training is a sequential process of many epochs that optimize network parameters. In one of such attempts, van Grinsven et al.<sup>199</sup> improved CNN training by dynamically selecting misclassified negative samples during training. In every epoch, they proposed to randomly select a subset of samples to update network parameters. As the majority of training samples are often highly correlated due to the repetitive pattern of normal tissues, only a small fraction of acquired images are informative. Thus, their approach to identify informative normal samples to use only a subset of samples for training not only improved the training efficiency but also speeded up the process. Another common approach in medical imaging to address the limited data challenge is to adopt transfer learning, where CNN models trained on natural image datasets or from a different medical domain are used. The CNN model is then fine-tuned as per the requirement of the task at hand, especially when a medium size dataset is available. Tajbakhsh et al. proposed in their study that using pretrained networks and fine-tuning them could provide much improved results, especially with smaller size datasets.<sup>106</sup> Their analysis further showed that deep fine-tuning led to improved performance over shallow fine-tuning.

Few-shot learning algorithms are another approach when dealing with limited datasets. These algorithms are especially very useful in image classification, and segmentation tasks can represent a small amount of data in such a way that it can be generalized to a broader range of data. The few shot problem is generally of the form of a  $k$ -shot  $n$ -way, where  $k$  refers to the number of available training samples, and  $n$  refers to number of classes the sample may belong to.<sup>200–202</sup> Matching networks,<sup>203</sup> prototyping networks,<sup>204</sup> and model agnostic meta-learning<sup>205</sup> are some recent advances in few-shot learning. However, these advancements have not yet been explored in ultrasound imaging (and consequently ultrasound elastography) and scopes remain open. Finally, it is also worth mentioning the federated learning approach to address data scarcity. The main idea in federated learning is to build AI models based on datasets that are distributed across multiple devices, while preventing data leakage. It involves a process in which a number of data owners who wish to train their AI model, collaboratively but without sharing the data, can do so without one owner's data getting exposed to others.<sup>206</sup> This is especially important when patients' data cannot be shared across multiple institutions due to confidentiality, ethical, or intellectual property-related issues. Improving data security remains the focus of the federated learning approach.

Before concluding, it is worth mentioning that deep models also have some limitations. Although deep learning methods have shown promise for wide biomedical applications, they are not yet popular and translated in clinical systems,<sup>207</sup> especially in ultrasound elastography, due to variability (e.g., signal-to-noise ratio, contrast-to-noise ratio, image resolution, and image outliers) caused by the data itself. Quantitative prediction of viscoelastic properties is not yet solved with deep learning. This may take a while due to the scarcity of labeled training datasets. In addition, data coming from systems manufactured by different vendors makes it further challenging and causes generalization gap.<sup>208</sup> Another challenge is that these models are usually trained for only one task (single imaging modality, specific tissue type, etc.) and cannot be easily generalized for different tasks. It is sure, AI will change radiology in the upcoming decades, and radiologists will gain considerable productivity benefits from integrating AI with their practice.<sup>146,209</sup>

Rigorous data collection criteria and uniform global ethical guidelines for AI need to be developed in order to establish its role in clinical practice and for advancing applications in elastography. Ethical and legal responsibilities for decision-making will remain under the responsibility of physicians and AI should adapt to this context. Although it has been well demonstrated that humans and AI models working together can achieve a higher level of accuracy in ultrasound elastography-based diagnosis and prognosis, efforts,

legislation strategies, and legal issues will have to be addressed to include AI into clinical guideline practices.

One common obstacle across research groups is that it is not easy for single sites to generate a large amount of data and to label it. Multicenter initiatives, collaborative research, data sharing, and crowd sourcing are some possible approaches to unite useful resources for further deep learning-based advancements in elastography. Although the lack of labeled data can be tackled with semi-supervised or unsupervised learning, one strategy to minimize the burden of manual labeling or annotations could be to use active learning, where the model selects uncertain predictions for manual correction before retraining.<sup>210</sup> Zhou et al.<sup>146</sup> called for creating a globally interconnected network of an open patient dataset to include diverse demographics and geographical locations. This would also promote AI research in countries where acquiring patient datasets is a challenge due to ethical, financial, or bureaucratic limitations. AI in medical research will only move forward in a socially responsible and globally beneficial way by promoting open access research and shared clinical datasets.

## ACKNOWLEDGMENTS

H. L. acknowledges the postdoctoral fellowship support of the TransMedTech Institute, École Polytechnique of Montréal. This work was partially funded by the postdoctoral start-up funds from the Canada First Research Excellence Fund through the TransMedTech Institute. This work was also partially funded by the Canadian Institutes of Health Research (Nos. 399544, 273738, 301520, and 134748), Fonds de Recherche du Québec (Nos. 2019-AUDC-263591), and Collaborative Health Research Program of the Natural Sciences and Engineering Research Council of Canada (No. 462240-14).

## CONFLICT OF INTEREST

The authors have no relevant conflicts of interest to disclose.

## REFERENCES

1. Ophir J, Cespedes I, Ponnekanti H, Yazdi Y, Li X. Elastography: a quantitative method for imaging the elasticity of biological tissues. *Ultrason Imaging*. 1991;13(2):111-134.
2. Turgay E, Salcudean S, Rohling R. Identifying the mechanical properties of tissue by ultrasound strain imaging. *Ultrasound Med Biol*. 2006;32(2):221-235.
3. Varghese T, Konofagou E, Ophir J, Alam S, Bilgen L. Direct strain estimation in elastography using spectral cross-correlation. *Ultrasound Med Biol*. 2000;26(9):1525-1537.
4. Jiang J, Hall TJ. A generalized speckle tracking algorithm for ultrasonic strain imaging using dynamic programming. *Ultrasound Med Biol*. 2009;35(11):1863-1879.
5. Lopata RG, Nillesen MM, Thijssen JM, Kapusta L, de Korte CL. Three-dimensional cardiac strain imaging in healthy children using RF-data. *Ultrasound Med Biol*. 2011;37(9):1399-1408.
6. Korukonda S, Doyley MM. Visualizing the radial and circumferential strain distribution within vessel phantoms using

- synthetic-aperture ultrasound elastography. *IEEE Trans Ultrason Ferroelectr Freq Control*. 2012;59(8):1639-1653.
7. Hansen H, Lopata R, de Korte CL. Noninvasive carotid strain imaging using angular compounding at large beam steered angles: validation in vessel phantoms. *IEEE Trans Med Imaging*. 2009;28(6):872-880.
  8. Maurice RL, Ohayon J, Fretigny Y, Bertrand M, Soulez G, Cloutier G. Noninvasive vascular elastography: theoretical framework. *IEEE Trans Med Imaging*. 2004;23(2):164-180.
  9. Luo J, Konofagou EE. High-frame rate, full-view myocardial elastography with automated contour tracking in murine left ventricles in vivo. *IEEE Trans Ultrason Ferroelectr Freq Control*. 2008;55(1):240-248.
  10. Catheline S, Wu F, Fink M. A solution to diffraction biases in sonoelasticity: the acoustic impulse technique. *J Acoust Soc Am*. 1999;105(5):2941-2950.
  11. Sarvazyan AP, Rudenko OV, Swanson SD, Fowlkes JB, Emelianov SY. Shear wave elasticity imaging: a new ultrasonic technology of medical diagnostics. *Ultrasound Med Biol*. 1998;24(9):1419-1435.
  12. Bercoff J, Tanter M, Fink M. Supersonic shear imaging: a new technique for soft tissue elasticity mapping. *IEEE Trans Ultrason Ferroelectr Freq Control*. 2004;51(4):396-409.
  13. Santos P, Petrescu AM, Pedrosa JP, et al. Natural shear wave imaging in the human heart: normal values, feasibility, and reproducibility. *IEEE Trans Ultrason Ferroelectr Freq Control*. 2019;66(3):442-452.
  14. Papadacci C, Finel V, Villemain O, Tanter M, Pernot M. 4D ultrafast ultrasound imaging of naturally occurring shear waves in the human heart. *IEEE Trans Med Imaging*. 2020;39(12):4436-4444.
  15. Salles S, Espeland T, Molares A, et al. 3D myocardial mechanical wave measurements: toward in vivo 3D myocardial elasticity mapping. *JACC Cardiovasc Imaging*. 2021;14(8):1495-1505.
  16. Krizhevsky A, Sutskever I, Hinton GE. ImageNet classification with deep convolutional neural networks. *Advances in Neural Information Processing Systems*. 2012:1097-1105.
  17. Ren S, He K, Girshick R, Sun J. Faster R-CNN: towards real-time object detection with region proposal networks. *IEEE Trans Pattern Anal Mach Intell*. 2017;39(6):1137-1149.
  18. Wang L, Liu T, Wang G, Chan KL, Yang Q. Video tracking using learned hierarchical features. *IEEE Trans Image Process*. 2015;24(4):1424-1435.
  19. Dong C, Loy CC, He K, Tang X. Image super-resolution using deep convolutional networks. *IEEE Trans Pattern Anal Mach Intell*. 2016;38(2):295-307.
  20. van Sloun RJG, Cohen R, Eldar YC. Deep learning in ultrasound imaging. *Proc IEEE*. 2020;108(1):11-29.
  21. Liu S, Wang Y, Yang X, et al. Deep learning in medical ultrasound analysis: a review. *Engineering*. 2019;5(2):261-275.
  22. Sridhar M, Liu J, Insana MF. Viscoelasticity imaging using ultrasound: parameters and error analysis. *Phys Med Biol*. 2007;52(9):2425-2443.
  23. Eskandari H, Salcudean SE, Rohling R. Viscoelastic parameter estimation based on spectral analysis. *IEEE Trans Ultrason Ferroelectr Freq Control*. 2008;55(7):1611-1125.
  24. Konofagou EE, D'hooge J, Ophir J. Myocardial elastography—a feasibility study in vivo. *Ultrasound Med Biol*. 2002;28(4):475-482.
  25. de Korte CL, van der Steen AF, Céspedes EI, et al. Characterization of plaque components and vulnerability with intravascular ultrasound elastography. *Phys Med Biol*. 2000;45(6):1465-1475.
  26. de Korte CL, Carlier SG, Mastik F, et al. Morphological and mechanical information of coronary arteries obtained with intravascular elastography: feasibility study in vivo. *Eur Heart J*. 2002;23(5):405-413.
  27. Poree J, Garcia D, Chayer B, Ohayon J, Cloutier G. Noninvasive vascular elastography with plane strain incompressibility assumption using ultrafast coherent compound plane wave imaging. *IEEE Trans Med Imaging*. 2015;34(12):2618-2631.
  28. Kanai H, Hasegawa H, Ichiki M, Tezuka F, Koiwa Y. Elasticity imaging of atheroma with transcutaneous ultrasound: preliminary study. *Circulation*. 2003;107(24):3018-3021.
  29. Li H, Porée J, Chayer B, Cardinal M-HR, Cloutier G. Parameterized strain estimation for vascular ultrasound elastography with sparse representation. *IEEE Trans Med Imaging*. 2020;39(12):3788-3800.
  30. Li H, Chayer B, Roy Cardinal M-H, et al. Investigation of out-of-plane motion artifacts in 2D noninvasive vascular ultrasound elastography. *Phys Med Biol*. 2018;63(24):245003.
  31. Anderson ME. Multi-dimensional velocity estimation with ultrasound using spatial quadrature. *IEEE Trans Ultrason Ferroelectr Freq Control*. 1998;45(3):852-861.
  32. Jensen JA, Munk P. A new method for estimation of velocity vectors. *IEEE Trans Ultrason Ferroelectr Freq Control*. 1998;45(3):886-894.
  33. Li H, Poree J, Roy Cardinal MH, Cloutier G. Two-dimensional affine model-based estimators for principal strain vascular ultrasound elastography with compound plane wave and transverse oscillation beamforming. *Ultrasonics*. 2019;91:77-91.
  34. Li H, Flé G, Bhatt M, et al. Viscoelasticity imaging of biological tissues and single cells using shear wave propagation. *Front Phys*. 2021;9:666192.
  35. Sigrüst RMS, Liau J, Kaffas AE, Chammas MC, Willmann JK. Ultrasound elastography: review of techniques and clinical applications. *Theranostics*. 2017;7(5):1303-1329.
  36. Tang A, Cloutier G, Szeverenyi NM, Sirlin CB. Ultrasound elastography and MR elastography for assessing liver fibrosis: Part 1, Principles and techniques. *AJR Am J Roentgenol*. 2015;205(1):22-32.
  37. Tang A, Cloutier G, Szeverenyi NM, Sirlin CB. Ultrasound elastography and MR elastography for assessing liver fibrosis: Part 2, Diagnostic performance, confounders, and future directions. *AJR Am J Roentgenol*. 2015;205(1):33-40.
  38. McAleavey SA, Menon M, Orszulak J. Shear-modulus estimation by application of spatially-modulated impulsive acoustic radiation force. *Ultrason Imaging*. 2007;29(2):87-104.
  39. Oestreicher HL. Field and impedance of an oscillating sphere in a viscoelastic medium with an application to biophysics. *J Acoust Soc Am*. 1951;23(6):707-714.
  40. Ophir J, Alam SK, Garra B, et al. Elastography: ultrasonic estimation and imaging of the elastic properties of tissues. *Proc Inst Mech Eng H*. 1999;213(3):203-233.
  41. Kazemirad S, Bernard S, Hybois S, Tang A, Cloutier G. Ultrasound shear wave viscoelastography: model-independent quantification of the complex shear modulus. *IEEE Trans Ultrason Ferroelectr Freq Control*. 2016;63(9):1399-1408.
  42. Lerner RM, Parker KJ, Holen J, Gramiak R, Waag RC. Sonoelasticity: medical elasticity images derived from ultrasound signals in mechanically vibrated targets. In *Acoustical Imaging*. Springer; 1988:317-327.
  43. Yamakoshi Y, Sato J, Sato T. Ultrasonic imaging of internal vibration of soft tissue under forced vibration. *IEEE Trans Ultrason Ferroelectr Freq Control*. 1990;37(2):45-53.
  44. Fatemi M, Greenleaf JF. Ultrasound-stimulated vibro-acoustic spectroscopy. *Science*. 1998;280(5360):82-85.
  45. Chen S, Urban MW, Pislaru C, et al. Shearwave dispersion ultrasound vibrometry (SDUV) for measuring tissue elasticity and viscosity. *IEEE Trans Ultrason Ferroelectr Freq Control*. 2009;56(1):55-62.
  46. Nightingale KR, Palmeri ML, Nightingale RW, Trahey GE. On the feasibility of remote palpation using acoustic radiation force. *J Acoust Soc Am*. 2001;110(1):625-634.
  47. Song P, Macdonald MC, Behler RH, et al. Two-dimensional shear-wave elastography on conventional ultrasound scanners with time-aligned sequential tracking (TAST) and comb-push

- ultrasound shear elastography (CUSE). *IEEE Trans Ultrason Ferroelectr Freq Control*. 2015;62(2):290-302.
48. Deffieux T, Gennisson J-L, Bousquet L, et al. Investigating liver stiffness and viscosity for fibrosis, steatosis and activity staging using shear wave elastography. *J Hepatol*. 2015;62(2):317-324.
  49. Lu J, Chen M, Chen Q-H, Wu Q, Jiang J-N, Leung T-Y. Elastogram: physics, clinical applications, and risks. *Matern-Fetal Med*. 2019;1(2):113-122.
  50. Barr RG. Liver elastography still in its infancy. *Radiology*. 2018;288(1):107-108.
  51. Barr RG. Future of breast elastography. *Ultrasonography*. 2019;38(2):93-105.
  52. Hwang SI, Lee HJ, Lee SE, Hong SK, Byun SS, Choe G. Elastographic strain index in the evaluation of focal lesions detected with transrectal sonography of the prostate gland. *J Ultrasound Med*. 2016;35(5):899-904.
  53. Zhang B, Ma X, Zhan W, et al. Real-time elastography in the diagnosis of patients suspected of having prostate cancer: a meta-analysis. *Ultrasound Med Biol*. 2014;40(7):1400-1407.
  54. Brock M, von Bodman C, Sommerer F, et al. Comparison of real-time elastography with grey-scale ultrasonography for detection of organ-confined prostate cancer and extra capsular extension: a prospective analysis using whole mount sections after radical prostatectomy. *BJU Int*. 2011;108(8b):E217-E222.
  55. Bojunga J, Herrmann E, Meyer G, Weber S, Zeuzem S, Friedrich-Rust M. Real-time elastography for the differentiation of benign and malignant thyroid nodules: a meta-analysis. *Thyroid*. 2010;20(10):1145-1150.
  56. Hairu L, Yulan P, Yan W, et al. Elastography for the diagnosis of high-suspicion thyroid nodules based on the 2015 American Thyroid Association guidelines: a multicenter study. *BMC Endocr Disord*. 2020;20(1):43.
  57. Samir AE, Dhyani M, Vij A, et al. Shear-wave elastography for the estimation of liver fibrosis in chronic liver disease: determining accuracy and ideal site for measurement. *Radiology*. 2015;274(3):888-896.
  58. Goddi A, Bonardi M, Alessi S. Breast elastography: a literature review. *J Ultrasound*. 2012;15(3):192-198.
  59. Evans A, Whelehan P, Thomson K, et al. Invasive breast cancer: relationship between shear-wave elastographic findings and histologic prognostic factors. *Radiology*. 2012;263(3):673-677.
  60. Barr RG, Memo R, Schaub CR. Shear wave ultrasound elastography of the prostate: initial results. *Ultrasound Q*. 2012;28(1):13-20.
  61. Sebag F, Vaillant-Lombard J, Berbis J, et al. Shear wave elastography: a new ultrasound imaging mode for the differential diagnosis of benign and malignant thyroid nodules. *J Clin Endocrinol Metab*. 2010;95(12):5281-5288.
  62. Davis LC, Baumer TG, Bey MJ, Holsbeeck MV. Clinical utilization of shear wave elastography in the musculoskeletal system. *Ultrasonography*. 2019;38(1):2-12.
  63. Brum J, Bernal M, Gennisson JL, Tanter M. In vivo evaluation of the elastic anisotropy of the human Achilles tendon using shear wave dispersion analysis. *Phys Med Biol*. 2014;59(3):505-523.
  64. Prado-Costa R, Rebelo J, Monteiro-Barroso J, Preto AS. Ultrasound elastography: compression elastography and shear-wave elastography in the assessment of tendon injury. *Insights Imaging*. 2018;9(5):791-814.
  65. Bhatia KS, Cho CC, Tong CS, Yuen EH, Ahuja AT. Shear wave elasticity imaging of cervical lymph nodes. *Ultrasound Med Biol*. 2012;38(2):195-201.
  66. Samir AE, Allegretti AS, Zhu Q, et al. Shear wave elastography in chronic kidney disease: a pilot experience in native kidneys. *BMC Nephrol*. 2015;16(1):1-9.
  67. Barr RG, De Silvestri A, Scotti V, et al. Diagnostic performance and accuracy of the 3 interpreting methods of breast strain elastography: a systematic review and meta-analysis. *J Ultrasound Med*. 2019;38(6):1397-1404.
  68. Jenssen C, Dietrich CF. Endoscopic ultrasound-guided fine-needle aspiration biopsy and Trucut biopsy in gastroenterology – an overview. *Best Pract Res Clin Gastroenterol*. 2009;23(5):743-759.
  69. Paterson S, Duthie F, Stanley AJ. Endoscopic ultrasound-guided elastography in the nodal staging of oesophageal cancer. *World J Gastroenterol*. 2012;18(9):889-895.
  70. Teng DK, Wang H, Lin YQ, Sui GQ, Guo F, Sun LN. Value of ultrasound elastography in assessment of enlarged cervical lymph nodes. *Asian Pac J Cancer Prev*. 2012;13(5):2081-2085.
  71. Varghese T, Ophir J. A theoretical framework for performance characterization of elastography: the strain filter. *IEEE Trans Ultrason Ferroelectr Freq Control*. 1997;44(1):164-172.
  72. Horn BK, Schunck BG. Determining optical flow. *Artif Intell*. 1981;17(1-3):185-203.
  73. Ni B, Gao H. A deep learning approach to the inverse problem of modulus identification in elasticity. *MRS Bull*. 2021;46(1):19-25.
  74. Goodfellow I, Bengio Y, Courville A. *Deep Learning*. MIT Press; 2016.
  75. Fenton JJ, Taplin SH, Carney PA, et al. Influence of computer-aided detection on performance of screening mammography. *N Engl J Med*. 2007;356(14):1399-1409.
  76. Litjens G, Kooi T, Bejnordi BE, et al. A survey on deep learning in medical image analysis. *Med Image Anal*. 2017;42:60-88.
  77. Barragan-Montero A, Javaid U, Valdes G, et al. Artificial intelligence and machine learning for medical imaging: a technology review. *Physica Med*. 2021;83:242-256.
  78. Yap MH, Pons G, Marti J, et al. Automated breast ultrasound lesions detection using convolutional neural networks. *IEEE J Biomed Health Inform*. 2018;22(4):1218-1226.
  79. Kooi T, Litjens G, van Ginneken B, et al. Large scale deep learning for computer aided detection of mammographic lesions. *Med Image Anal*. 2017;35:303-312.
  80. Ronneberger O, Fischer P, Brox T. U-net: convolutional networks for biomedical image segmentation. International Conference on Medical Image Computing and Computer-Assisted Intervention. 2015:234-241.
  81. Huynh B, Drukker K, Giger M. MO-DE-207B-06: computer-aided diagnosis of breast ultrasound images using transfer learning from deep convolutional neural networks. *Med Phys*. 2016;43(6):3705-3705.
  82. Ravishankar H, Sudhakar P, Venkataramani R, et al. Understanding the mechanisms of deep transfer learning for medical images. *Deep Learning and Data Labeling for Medical Applications*. Springer; 2016:188-196.
  83. Wildeboer RR, van Sloun RJG, Mannaerts CK, et al. Synthetic elastography using B-mode ultrasound through a deep fully convolutional neural network. *IEEE Trans Ultrason Ferroelectr Freq Control*. 2020;67(12):2640-2648.
  84. Chen J, Yang L, Zhang Y, Alber M, Chen DZ. Combining fully convolutional and recurrent neural networks for 3d biomedical image segmentation. In: *Advances in Neural Information Processing Systems*. Curran Associates Inc., Red Hook, NY, USA; 2016:3036-3044.
  85. Azizi S, Bayat S, Yan P, et al. Deep recurrent neural networks for prostate cancer detection: analysis of temporal enhanced ultrasound. *IEEE Trans Med Imaging*. 2018;37(12):2695-2703.
  86. Marquez ES, Hare JS, Niranjan M. Deep cascade learning. *IEEE Trans Neural Netw Learn Syst*. 2018;29(11):5475-5485.
  87. Schlemper J, Caballero J, Hajnal JV, Price AN, Rueckert D. A deep cascade of convolutional neural networks for dynamic MR image reconstruction. *IEEE Trans Med Imaging*. 2018;37(2):491-503.
  88. Peng B, Xian Y, Xian Y. A convolution neural network-based speckle tracking method for ultrasound elastography. IEEE International Ultrasonics Symposium. 2018:206-212.

89. Pan Z, Yu W, Yi X, Khan A, Yuan F, Zheng Y. Recent progress on generative adversarial networks (GANs): a survey. *IEEE Access*. 2019;7:36322-36333.
90. Goodfellow IJ, Pouget-Abadie J, Mirza M, et al. Generative adversarial nets. *Advances in Neural Information Processing Systems*. 2014:2672-2680.
91. Zhu J-Y, Park T, Isola P, Efros AA. Unpaired image-to-image translation using cycle-consistent adversarial networks. *IEEE International Conference on Computer Vision*. 2017:2223-2232.
92. Kazemini S, Baur C, Kuijper A, et al. GANs for medical image analysis. *Artif Intell Med*. 2020;109:101938.
93. Armanious K, Jiang C, Fischer M, et al. MedGAN: medical image translation using GANs. *Comput Med Imaging Graph*. 2020;79:101684.
94. Skandarani Y, Jodoin P-M, Lalonde A. GANs for medical image synthesis: an empirical study. 2021. arXiv preprint arXiv: 2105.05318.
95. Tehrani AK, Mirzaei M, Rivaz H. Semi-supervised training of optical flow convolutional neural networks in ultrasound elastography. *International Conference on Medical Image Computing and Computer-Assisted Intervention*. Springer; 2020:504-513.
96. Khan S, Huh J, Ye JC. Variational formulation of unsupervised deep learning for ultrasound image artifact removal. *IEEE Trans Ultrason Ferroelectr Freq Control*. 2021;68(6):2086-2100.
97. Brattain LJ, Telfer BA, Dhyani M, Grajo JR, Samir AE. Machine learning for medical ultrasound: status, methods, and future opportunities. *Abdom Radiol*. 2018;43(4):786-799.
98. Delaunay R, Hu Y, Vercauteren T. An unsupervised approach to ultrasound elastography with end-to-end strain regularisation. *International Conference on Medical Image Computing and Computer-Assisted Intervention*. Springer; 2020:573-582.
99. Ma K, Wang J, Singh V, et al. Multimodal image registration with deep context reinforcement learning. *International Conference on Medical Image Computing and Computer-Assisted Intervention*. Springer; 2017:240-248.
100. Coronato A, Naeem M, De Pietro G, Paragliola G. Reinforcement learning for intelligent healthcare applications: a survey. *Artif Intell Med*. 2020;109:101964.
101. Hase H, Azampour MF, Tirindelli M, et al. Ultrasound-guided robotic navigation with deep reinforcement learning. 2020 IEEE/RSJ International Conference on Intelligent Robots and Systems (IROS). 2020:5534-5541.
102. Liu T, Meng Q, Vlontzos A, Tan J, Rueckert D, Kainz B. Ultrasound video summarization using deep reinforcement learning. *International Conference on Medical Image Computing and Computer-Assisted Intervention*. Springer; 2020:483-492.
103. Li K, Wang J, Xu Y, Qin H, Liu D, Meng MQ-H. Autonomous navigation of an ultrasound probe towards standard scan planes with deep reinforcement learning. *IEEE International Conference on Robotics and Automation*. 2021:8302-8308.
104. Jarosik P, Lewandowski M. Automatic ultrasound guidance based on deep reinforcement learning. *IEEE International Ultrasonics Symposium (IUS)*. 2019:475-478.
105. Pan SJ, Yang Q. A survey on transfer learning. *IEEE Trans Knowl Data Eng*. 2009;22(10):1345-1359.
106. Tajbakhsh N, Shin JY, Gurudu SR, et al. Convolutional neural networks for medical image analysis: full training or fine tuning? *IEEE Trans Med Imaging*. 2016;35(5):1299-1312.
107. Simonyan K, Zisserman A. Very deep convolutional networks for large-scale image recognition. 2014. arXiv preprint arXiv:1409.1556.
108. He K, Zhang X, Ren S, Sun J. Deep residual learning for image recognition. *IEEE Conference on Computer Vision and Pattern Recognition*. 2016:770-778.
109. Szegedy C, Liu W, Jia Y, et al. Going deeper with convolutions. *IEEE Conference on Computer Vision and Pattern Recognition*. 2015:1-9.
110. Huang G, Liu Z, Maaten LVD, Weinberger KQ. Densely connected convolutional networks. *IEEE Conference on Computer Vision and Pattern Recognition*. 2017:4700-4708.
111. Joseph R, Santosh D, Ross G, Ali F. Proceedings of the IEEE Conference on Computer Vision and Pattern Recognition (CVPR). 2016:779-788.
112. Goodfellow I, Pouget-Abadie J, Mirza M, et al. Generative adversarial networks. *International Conference on Neural Information Processing Systems*. 2014:2672-2680.
113. Koch G, Zemel R, Salakhutdinov R. Siamese neural networks for one-shot image recognition. *ICML Deep Learning Workshop*. 2015:2.
114. Milletari F, Navab N, Ahmadi S. V-net: fully convolutional neural networks for volumetric medical image segmentation. *Fourth International Conference on 3D Vision (3DV)*. 2016:565-571.
115. Sutskever I, Martens J, Dahl G, Hinton G. On the importance of initialization and momentum in deep learning. *International Conference on Machine Learning*. 2013:1139-1147.
116. Kingma DP, Ba JL. Adam: a method for stochastic optimization. *International Conference on Learning Representations*. 2015.
117. Nair V, Hinton GE. Rectified linear units improve restricted Boltzmann machines. *International Conference on Machine Learning*. 2010:807-814.
118. Goodfellow IJ, Warde-Farley D, Mirza M, Courville A, Bengio Y. Maxout networks. *International Conference on Machine Learning*. 2013:1319-1327.
119. Srivastava N, Hinton G, Krizhevsky A, Sutskever I, Salakhutdinov R. Dropout: a simple way to prevent neural networks from overfitting. *J Mach Learn Res*. 2014;15(1):1929-1958.
120. Ioffe S, Szegedy C. Batch normalization: accelerating deep network training by reducing internal covariate shift. *International Conference on Machine Learning*. 2015:448-456.
121. Shang W, Sohn K, Almeida D, Lee H. Understanding and improving convolutional neural networks via concatenated rectified linear units. *International Conference on Machine Learning*. 2016:2217-2225.
122. Aggarwal HK, Mani MP, Jacob M. MoDL: model-based deep learning architecture for inverse problems. *IEEE Trans Med Imaging*. 2019;38(2):394-405.
123. Lee SA, Konofagou EE. FUS-net: u-Net-based FUS interference filtering. *IEEE Trans Med Imaging*. 2022;41:915-924.
124. Wu S, Gao Z, Luo J, Liu Z, Zhang H, Li S. Direct reconstruction of ultrasound elastography using an end-to-end deep neural network. *International Conference on Medical Image Computing and Computer-Assisted Intervention*. 2018:374-382.
125. Byra M, Styczynski G, Szmigielski C, et al. Transfer learning with deep convolutional neural network for liver steatosis assessment in ultrasound images. *Int J Comput Assist Radiol Surg*. 2018;13(12):1895-1903.
126. Xue LY, Jiang ZY, Fu TT, et al. Transfer learning radiomics based on multimodal ultrasound imaging for staging liver fibrosis. *Eur Radiol*. 2020;30(5):2973-2983.
127. Peng B, Huang X, Wang S, Jiang J. A real-time medical ultrasound simulator based on a generative adversarial network model. Presented at the IEEE International Conference on Image Processing (ICIP). 2019.
128. Zhou Z, Wang Y, Guo Y, Qi Y, Yu J. Image quality improvement of hand-held ultrasound devices with a two-stage generative adversarial network. *IEEE Trans Biomed Eng*. 2020;67(1):298-311.
129. Patel D, Tibrewala R, Vega A, Dong L, Hugenberg N, Oberai AA. Circumventing the solution of inverse problems in mechanics through deep learning: application to elasticity imaging. *Comput Methods Appl Mech Eng*. 2019;353:448-466.
130. Fischer P, Dosovitskiy A, Ilg E, et al. FlowNet: learning optical flow with convolutional networks. *Proceedings of the IEEE International Conference on Computer Vision*. 2015:2758-2766.

131. Ilg E, Mayer N, Saikia T, Keuper M, Dosovitskiy A, Brox T. FlowNet 2.0: evolution of optical flow estimation with deep networks. Proceedings of the IEEE Conference on Computer Vision and Pattern Recognition. 2017:2462-2470.
132. Ranjan A, Black MJ. Optical flow estimation using a spatial pyramid network. Proceedings of the IEEE Conference on Computer Vision and Pattern Recognition. 2017:4161-4170.
133. Hui T-W, Tang X, Tang X. LiteFlowNet: a lightweight convolutional neural network for optical flow estimation. Proceedings of the IEEE Conference on Computer Vision and Pattern Recognition. 2018:8981-8989.
134. Sun D, Yang X, Liu M-Y, Kautz J. PWC-Net: cNNs for optical flow using pyramid, warping, and cost Volume. Proceedings of the IEEE Conference on Computer Vision and Pattern Recognition. 2018:8934-8943.
135. Kibria MG, Rivaz H. GLUENet: ultrasound elastography using convolutional neural network. Simulation, Image Processing, and Ultrasound Systems for Assisted Diagnosis and Navigation. 2018:21-28.
136. Tehrani AKZ, Rivaz H. Displacement estimation in ultrasound elastography using pyramidal convolutional neural network. *IEEE Trans Ultrason Ferroelectr Freq Control*. 2020;67(12):2629-2639.
137. Peng B, Xian Y, Zhang Q, Jiang J. Neural network-based motion tracking for breast ultrasound strain elastography: an initial assessment of performance and feasibility. *Ultrason Imaging*. 2020;45(2):74-91.
138. Gao Z, Wu S, Liu Z, et al. Learning the implicit strain reconstruction in ultrasound elastography using privileged information. *Med Image Anal*. 2019;58:101534.
139. Østvik A, Smistad E, Espeland T, Berg EAR, Lovstakken L. Automatic myocardial strain imaging in echocardiography using deep learning. In *Deep Learning in Medical Image Analysis and Multimodal Learning for Clinical Decision Support*. Springer; 2018:309-316.
140. Ostvik A, Salte IM, Smistad E, et al. Myocardial function imaging in echocardiography using deep learning. *IEEE Trans Med Imaging*. 2021;40(5):1340-1351.
141. Alessandrini M, Chakraborty B, Heyde B, et al. Realistic vendor-specific synthetic ultrasound data for quality assurance of 2-D speckle tracking echocardiography: simulation pipeline and open access database. *IEEE Trans Ultrason Ferroelectr Freq Control*. 2018;65(3):411-422.
142. Lu A, Zontak M, Parajuli N, et al. Learning-based spatiotemporal regularization and integration of tracking methods for regional 4D cardiac deformation analysis. International Conference on Medical Image Computing and Computer-Assisted Intervention. 2017:323-331.
143. Lu A, Ahn SS, Ta K, et al. Learning-based regularization for cardiac strain analysis via domain adaptation. *IEEE Trans Med Imaging*. 2021;40(9):2233-2245.
144. Zhang Q, Xiao Y, Dai W, et al. Deep learning based classification of breast tumors with shear-wave elastography. *Ultrasonics*. 2016;72:150-157.
145. Zhang Q, Song S, Xiao Y, Chen S, Shi J, Zheng H. Dual-mode artificially-intelligent diagnosis of breast tumours in shear-wave elastography and B-mode ultrasound using deep polynomial networks. *Med Eng Phys*. 2019;64:1-6.
146. Zhou LQ, Wang JY, Yu SY, et al. Artificial intelligence in medical imaging of the liver. *World J Gastroenterol*. 2019;25(6):672-682.
147. Wang K, Lu X, Zhou H, et al. Deep learning Radiomics of shear wave elastography significantly improved diagnostic performance for assessing liver fibrosis in chronic hepatitis B: a prospective multicentre study. *Gut*. 2019;68(4):729-741.
148. Le Berre C, Sandborn WJ, Aridhi S, et al. Application of artificial intelligence to gastroenterology and hepatology. *Gastroenterology*. 2020;158(1):76-94.e2.
149. Qin P, Wu K, Hu Y, Zeng J, Chai X. Diagnosis of benign and malignant thyroid nodules using combined conventional ultrasound and ultrasound elasticity imaging. *IEEE J Biomed Health Inform*. 2020;24(4):1028-1036.
150. Gao J, Xu L, Bouakaz A, Wan M. A deep Siamese-based plantar fasciitis classification method using shear wave elastography. *IEEE Access*. 2019;7:130999-131007.
151. Wildeboer RR, Mannaerts CK, van Sloun RJG, et al. Automated multiparametric localization of prostate cancer based on B-mode, shear-wave elastography, and contrast-enhanced ultrasound radiomics. *Eur Radiol*. 2020;30(2):806-815.
152. Zhou Y, Xu J, Liu Q, et al. A radiomics approach with CNN for shear-wave elastography breast tumor classification. *IEEE Trans Biomed Eng*. 2018;65(9):1935-1942.
153. Yeo SH, Kim GR, Lee SH, Moon WK. Comparison of ultrasound elastography and color Doppler ultrasonography for distinguishing small triple-negative breast cancer from fibroadenoma. *J Ultrasound Med*. 2018;37(9):2135-2146.
154. Xiao Y, Zeng J, Niu L, et al. Computer-aided diagnosis based on quantitative elastographic features with supersonic shear wave imaging. *Ultrasound Med Biol*. 2014;40(2):275-286.
155. Zhang YN, Fowler KJ, Ozturk A, et al. Liver fibrosis imaging: a clinical review of ultrasound and magnetic resonance elastography. *J Magn Reson Imaging*. 2020;51(1):25-42.
156. Treacher A, Beauchamp D, Quadri B, et al. Deep learning convolutional neural networks for the estimation of liver fibrosis severity from ultrasound texture. *Proc SPIE Int Soc Opt Eng*. 2019;10950:109503E.
157. Nishida N, Yamakawa M, Shiina T, Kudo M. Current status and perspectives for computer-aided ultrasonic diagnosis of liver lesions using deep learning technology. *Hepatol Int*. 2019;13(4):416-421.
158. Liu X, Song JL, Wang SH, Zhao JW, Chen YQ. Learning to diagnose cirrhosis with liver capsule guided ultrasound image classification. *Sensors*. 2017;17(1):149.
159. Meng D, Zhang L, Cao G, Cao W, Zhang G, Hu B. Liver fibrosis classification based on transfer learning and FCNet for ultrasound images. *IEEE Access*. 2017;5:5804-5810.
160. Biswas M, Kupplili V, Edla DR, et al. Symtosis: a liver ultrasound tissue characterization and risk stratification in optimized deep learning paradigm. *Comput Methods Programs Biomed*. 2018;155:165-177.
161. Akkus Z, Cai J, Boonrod A, et al. A survey of deep-learning applications in ultrasound: artificial intelligence-powered ultrasound for improving clinical workflow. *J Am Coll Radiol*. 2019;16(9):1318-1328.
162. Gatos I, Tsantis S, Spiliopoulos S, et al. A machine-learning algorithm toward color analysis for chronic liver disease classification, employing ultrasound shear wave elastography. *Ultrasound Med Biol*. 2017;43(9):1797-1810.
163. Wei R, Wang J, Wang X, et al. Clinical prediction of HBV and HCV related hepatic fibrosis using machine learning. *EBioMedicine*. 2018;35:124-132.
164. Kagadis GC, Drazinos P, Gatos I, et al. Deep learning networks on chronic liver disease assessment with fine-tuning of shear wave elastography image sequences. *Phys Med Biol*. 2020;65(21):215027.
165. Brattain LJ, Ozturk A, Telfer BA, Dhyani M, Grajo JR, Samir AE. Image processing pipeline for liver fibrosis classification using ultrasound shear wave elastography. *Ultrasound Med Biol*. 2020;46(10):2667-2676.
166. Jin J, Yao Z, Zhang T, et al. Deep learning radiomics model accurately predicts hepatocellular carcinoma occurrence in chronic hepatitis B patients: a five-year follow-up. *Am J Cancer Res*. 2021;11(2):576.
167. Gatos I, Tsantis S, Spiliopoulos S, et al. Temporal stability assessment in shear wave elasticity images validated by deep

- learning neural network for chronic liver disease fibrosis stage assessment. *Med Phys*. 2019;46(5):2298-2309.
168. Nguyen DT, Pham TD, Batchuluun G, Yoon HS, Park KR. Artificial intelligence-based thyroid nodule classification using information from spatial and frequency domains. *J Clin Med*. 2019;8(11):1976.
169. Ma J, Wu F, Zhu J, Xu D, Kong D. A pre-trained convolutional neural network based method for thyroid nodule diagnosis. *Ultrasonics*. 2017;73:221-230.
170. Peng S, Liu Y, Lv W, et al. Deep learning-based artificial intelligence model to assist thyroid nodule diagnosis and management: a multicentre diagnostic study. *Lancet Digital Health*. 2021;3(4):e250-e259.
171. Zhou H, Jin Y, Dai L, et al. Differential diagnosis of benign and malignant thyroid nodules using deep learning radiomics of thyroid ultrasound images. *Eur J Radiol*. 2020;127:108992.
172. Saftoiu A, Vilmann P, Gorunescu F, et al. Efficacy of an artificial neural network-based approach to endoscopic ultrasound elastography in diagnosis of focal pancreatic masses. *Clin Gastroenterol Hepatol*. 2012;10(1):84-90.
173. Fujioka T, Katsuta L, Kubota K, et al. Classification of breast masses on ultrasound shear wave elastography using convolutional neural networks. *Ultrasonic Imaging*. 2020;42(4-5):213-220.
174. Zheng X, Yao Z, Huang Y, et al. Deep learning radiomics can predict axillary lymph node status in early-stage breast cancer. *Nat Commun*. 2020;11(1):1-9.
175. Nair AA, Washington KN, Tran TD, Reiter A, Bell MAL. Deep learning to obtain simultaneous image and segmentation outputs from a single input of raw ultrasound channel data. *IEEE Trans Ultrason Ferroelectr Freq Control*. 2020;67(12):2493-2509.
176. Wang G. A perspective on deep imaging. *IEEE Access*. 2016;4:8914-8924.
177. Chen L-C, Papandreou G, Schroff F, Adam H. Rethinking atrous convolution for semantic image segmentation. 2017. arXiv preprint arXiv:1706.05587.
178. Yap MH, Goyal M, Osman FM, et al. Breast ultrasound lesions recognition: end-to-end deep learning approaches. *J Med Imaging*. 2018;6(1):011007.
179. Isola P, Zhu J-Y, Zhou T, Efros AA. Image-to-image translation with conditional adversarial networks. IEEE Conference on Computer Vision and Pattern Recognition. 2017:1125-1134.
180. Park J, Hwang D, Kim KY, Kang SK, Kim YK, Lee JS. Computed tomography super-resolution using deep convolutional neural network. *Phys Med Biol*. 2018;63(14):145011.
181. He L, Peng B, Yang T, Jiang J. An application of super-resolution generative adversary networks for quasi-static ultrasound strain elastography: a feasibility study. *IEEE Access*. 2020;8:65769-65779.
182. Rajalingam B, Priya R. Multimodal medical image fusion based on deep learning neural network for clinical treatment analysis. *Int J ChemTech Res*. 2018;11(06):160-176.
183. Hermessi H, Mourali O, Zagrouba E. Convolutional neural network-based multimodal image fusion via similarity learning in the shearlet domain. *Neural Comput Appl*. 2018;30(7):2029-2045.
184. Ling RL. A computer generated aid for cluster analysis. *Commun ACM*. 1973;16(6):355-361.
185. Gasse M, Millioz F, Roux E, Garcia D, Liebgott H, Friboulet D. High-quality plane wave compounding using convolutional neural networks. *IEEE Trans Ultrason Ferroelectr Freq Control*. 2017;64(10):1637-1639.
186. Awasthi N, Prabhakar KR, Kalva SK, Pramanik M, Babu RV, Yalavarthy PK. PA-Fuse: deep supervised approach for the fusion of photoacoustic images with distinct reconstruction characteristics. *Biomed Opt Express*. 2019;10(5):2227-2243.
187. Gutta S, Kadimesetty VS, Kalva SK, Pramanik M, Ganapathy S, Yalavarthy PK. Deep neural network-based bandwidth enhancement of photoacoustic data. *J Biomed Opt*. 2017;22(11):1-7.
188. Hall TJ, Milkowski A, Garra B, et al. RSNA/QIBA: shear wave speed as a biomarker for liver fibrosis staging. 2013 IEEE International Ultrasonics Symposium (IUS). IEEE; 2013:397-400.
189. Palmeri M. RSNA/QIBA efforts to standardize shear wave speed as a biomarker for liver fibrosis staging. *Ultrasound Med Biol*. 2019;45:S24.
190. Shiina T, Nightingale KR, Palmeri ML, et al. WFUMB guidelines and recommendations for clinical use of ultrasound elastography: Part 1: Basic principles and terminology. *Ultrasound Med Biol*. 2015;41(5):1126-1147.
191. Dietrich CF, Bamber J, Berzigotti A, et al. EFSUMB guidelines and recommendations on the clinical use of liver ultrasound elastography, update 2017 (long version). *Ultraschall Med*. 2017;38(04):e16-e47.
192. Zhang Q, Suo J, Chang W, Shi J, Chen M. Dual-modal computer-assisted evaluation of axillary lymph node metastasis in breast cancer patients on both real-time elastography and B-mode ultrasound. *Eur J Radiol*. 2017;95:66-74.
193. Lopez MM, Frederick JM, Ventura J. Evaluation of MRI denoising methods using unsupervised learning. *Front Artif Intell*. 2021;4:642731.
194. Ghodrati V, Bydder M, Ali F, et al. Retrospective respiratory motion correction in cardiac cine MRI reconstruction using adversarial autoencoder and unsupervised learning. *NMR Biomed*. 2021;34(2):e4433.
195. Liang X, Chen L, Nguyen D, et al. Generating synthesized computed tomography (CT) from cone-beam computed tomography (CBCT) using CycleGAN for adaptive radiation therapy. *Phys Med Biol*. 2019;64(12):125002.
196. Sim B, Oh G, Kim J, Jung C, Ye JC. Optimal transport driven CycleGAN for unsupervised learning in inverse problems. *SIAM J Imaging Sci*. 2020;13(4):2281-2306.
197. Li Y, Li W, Xiong J, Xia J, Xie Y. Comparison of supervised and unsupervised deep learning methods for medical image synthesis between computed tomography and magnetic resonance images. *BioMed Res Int*. 2020;2020:5193707.
198. Parisi GI, Kemker R, Part JL, Kanan C, Wermter S. Continual lifelong learning with neural networks: a review. *Neural Netw*. 2019;113:54-71.
199. van Grinsven MJ, van Ginneken B, Hoyng CB, Theelen T, Sanchez CI. Fast convolutional neural network training using selective data sampling: application to hemorrhage detection in color fundus images. *IEEE Trans Med Imaging*. 2016;35(5):1273-1284.
200. Kotia J, Kotwal A, Bharti R, Mangrulkar R. Few shot learning for medical imaging. In: *Machine Learning Algorithms for Industrial Applications*. Springer; 2021:107-132.
201. Sun Q, Liu Y, Chua T-S, Schiele B. Meta transfer learning for few-shot learning. Conference on Computer Vision and Pattern Recognition. 2019:403-412.
202. Zhang R, Che T, Grahahramani Z, Bengio Y, Song Y. MetaGAN: an adversarial approach to few-shot learning. *Neural Inf Process Syst*. 2018;2:8.
203. Vinyals O, Blundell C, Lillicrap T, Kavukcuoglu K, Wierstra D. Matching networks for one shot learning. *Adv Neural Inf Process Syst*. 2016;29:3630-3638.
204. Snell J, Swersky K, Zemel RS. Prototypical networks for few-shot learning. 31st Conference on Neural Information Processing Systems. 2017. arXiv preprint arXiv: 1703.05175.
205. Finn C, Abbeel P, Levine S. Model-agnostic meta-learning for fast adaptation of deep networks. International Conference on Machine Learning. 2017:1126-1135.

206. Yang Q, Liu Y, Chen T, Tong Y. Federated machine learning: concept and applications. *ACM Trans Intell Syst.* 2019;10(2):1-19.
207. Miotto R, Wang F, Wang S, Jiang X, Dudley JT. Deep learning for healthcare: review, opportunities and challenges. *Brief Bioinform.* 2018;19(6):1236-1246.
208. Perone CS, Cohen-Adad J. Promises and limitations of deep learning for medical image segmentation. *J Med Artif Intell.* 2019;2(1):1-2.
209. Pesapane F, Codari M, Sardanelli F. Artificial intelligence in medical imaging: threat or opportunity? Radiologists again at the forefront of innovation in medicine. *Eur Radiol Exp.* 2018;2(1):1-10.
210. Wang K, Zhang D, Li Y, Zhang R, Lin L. Cost-effective active learning for deep image classification. *IEEE Trans Circuits Syst Video Technol.* 2017;27(12):2591-2600.

**How to cite this article:** Li H, Bhatt M, Qu Z, et al. Deep learning in ultrasound elastography imaging: A review. *Med Phys.* 2022;49:5993–6018.  
<https://doi.org/10.1002/mp.15856>